Insights into the evolution of the Hindu Kush-Kohistan-Karakoram from modern river sand detrital geo- and thermochronological studies

Guangsheng Zhuang[1, *], Yani Najman[2, *], Yuntao Tian[3], Andrew Carter[4], Lorenzo Gemignani[5], Jan Wijbrans[5], M. Qasim Jan[6], and M. Asif Khan[6]

[1] Department of Geology and Geophysics, Louisiana State University, Baton Rouge, LA 70803, USA

[2] Lancaster Environment Centre, Lancaster University, LA1 4YQ, Lancaster, UK

[3] School of Earth Sciences and Engineering, Sun Yat-sen University, Guangzhou, 510275 China

[4] Department of Earth and Planetary Sciences, Birkbeck, University of London, London WC1E 7HX, UK

[5] Department of Isotope Geology, Vrije Universiteit, De Boelelaan 1085, 1081 Amsterdam, Netherlands

[6] National Centre of Excellence in Geology, University of Peshawar, Peshawar 25130, Pakistan.

[*] gzhuang@lsu.edu, y.najman@lancaster.ac.uk

Abstract:

The Hindu Kush-Kohistan-Karakoram region is critical to understanding the long-term accretion history of the south Asian margin pre- and post-India-Asia collision and the impact of these collisions on the development of high topography. However, knowledge about this region remains incomplete due to sparse studies. Here, we present a study comprising detrital zircon U-Pb geochronology, detrital muscovite $^{40}Ar/^{39}Ar$ thermochronology, and numerical modeling on $^{40}Ar/^{39}Ar$ dates. The study identifies zircon U-Pb age peaks at 200 Ma, 110–130 Ma, 60–80 Ma, and 28–40 Ma, supporting the polyphase collisions and crustal growth in the south Asian margin. Modeling study reveals fast cooling/erosion at 115–129 Ma, 69–71 Ma, 27–35 Ma, and < 8 Ma, which are synchronous with collision related crustal growth, indicating the significant impact of accretion both prior to and post India-Asia collision. This study, along with studies in eastern Karakoram, reveals along-strike variations in erosion and exhumation with young (since late Miocene) intense erosion focusing on the east-central Karakoram. We suggest that this east-west spatial variation in exhumation may have been associated with more intense crustal shortening, and thus the greater crustal thickness, topographic relief and altitude observed in the eastern, compared to western, Karakoram.

1. Introduction

The Himalaya-Tibetan Plateau is an archetype for understanding orogenesis associated with continent-continent collision (e.g. Burchfiel et al., 1989; Molnar and Tapponnier, 1975; Tapponnier et al., 1982). The western Himalaya-Tibetan Plateau—including the Hindu Kush, Kohistan, and Karakoram (Fig.1A)—is of particular interest to the study of geodynamic processes because of its protracted convergence and accretion history.

During the Mesozoic Cimmerian Orogeny, a number of micro-continents which had drifted away from Gondwana successively collided with Asia (e.g. Angiolini et al., 2013; Gaetani et al., 1993; Qasim et al., 2017; Robinson, 2015; Zanchi and Gaetani, 2011), culminating with the final India-Asia collision and Himalayan inception at ca. 60–50 Ma (Hu et al., 2016 and references therein). Various episodes of crustal thickening and exhumation have also been documented in the northwestern Himalaya and Karakoram following the India-Asia collision (e.g. Carter et al., 2010; Cerveny et al., 1989; Dunlap et al., 1998; Foster et al., 1994; Krol et al., 1996a; Krol et al., 1996b; Schneider et al., 2001; Van Der Beek et al., 2009; Wallis et al., 2016; Zeitler et al., 2001). Whilst the exhumation history since the India-Asia collision is reasonably well documented in the eastern Karakoram and Nanga Parbat region, little is known regarding this region’s geological history prior to the India-Asia collision and farther to the west. Such information is important since it allows insight into the degree of elevation that may have existed in the now elevated southern margin of the Asian plate prior to India-Asia collision, thus impacting models of crustal deformation.

The east-central Karakoram generally has high topography (> 5 km) characterized by extreme relief (> 6 to 7 km), deeply eroded and exposed deep crustal materials (Searle, 2015), and thick crust (>70–80 km) (e.g. Hazarika et al., 2014; Holt and Wallace, 1990; Rai et al., 2006; Wittlinger et al., 2004). Using apatite fission track analysis, Wallis et al. (2016) identified a rapid phase of exhumation at 7–3 Ma in the eastern Karakoram, which follows a northward increasing trend across the Indus suture zone from the Ladakh arc to the Karakoram. Although the study region is located close to the major Karakoram Fault (Fig. 1B), Wallis et al. (2016) argue for their data to be explained by a large-scale regional tectonic driver which was responding to substantial crustal thickening in the Karakoram, with consequent elevation gain leading to increased glaciation and thus enhanced exhumation. Other studies in close proximity to the Karakoram Fault (Fig. 1B) reveal similar observations of late Miocene-Pliocene rapid cooling associated with tectonic and/or erosional processes (e.g. Cerveny et al., 1989; Foster et al., 1994; Krol et al., 1996b). Whether this rapid exhumation pattern is similar in the western Karakoram and thus how the driver may vary across the region remains unknown.

Documentation of the exhumation history of the Karakoram adds to the growing database used to understand downstream palaeo-drainage evolution. Previous work on the sedimentary rocks deposited by the paleo-Indus in the Himalayan foreland and in the Indus Fan reveals a marked shift in geochemical signal since the late Miocene, which has been attributed to either major re-routing of Himalayan tributaries from eastward into the Ganges to westward into the Indus system (Clift and Blusztajn, 2005), or enhanced exhumation of the Karakoram (Chirouze et al., 2015). Better understanding of the timing of Karakoram exhumation will allow discrimination between these models.

In constraining the spatial-temporal exhumation history and driving forces of the western Himalaya and Tibetan Plateau, both bedrock and detrital studies have previously been used. Bedrock vertical transect studies, so called "in situ thermochronology" (Braun et al., 2006), demonstrate the utility of densely sampling basement rocks (intervals of 100s meters in vertical scale) along with thermal modeling, which provide extra information on particle trajectories during exhumation towards the surface (e.g. Foster et al., 1994; Van Der Beek et al., 2009; Wallis et al., 2016). Whilst these studies have high spatial resolution, the ability of vertical transect studies is limited in temporal range due to the loss of old rocks at structurally high horizons which have been removed during the earlier stages of orogenesis; such rocks contain critical information about tectonism and erosion beyond the present-day mountain belt (Braun et al., 2006; Clift et al., 2004). Hence, a substantial amount of effort in thermochronology has also been focused on the products of erosion, i.e. the detritus present in fluvial systems and preserved in the receiving basins, which has greatly extended the temporal record of orogenesis (Braun et al., 2006; Cerveny et al., 1989; Clift et al., 2004; Garver et al., 1999; Najman et al., 2008; Reiners and Brandon, 2006).

To evaluate the regional variations in exhumation and to extend the temporal range in order to better understand the long-term evolution of the region, we undertook a detrital study based on muscovite $^{40}Ar/^{39}Ar$ thermochronology on modern river sediments. The closure temperature of muscovite $^{40}Ar/^{39}Ar$ thermochronology is >350 °C (McDougall and Harrison, 1999). With a geothermal gradient of 15 to 30 °C/km (typical for young and old orogen), the closure temperature suggests that muscovite $^{40}Ar/^{39}Ar$ thermochronology can detect crustal exhumation processes from 10 to 20 km. We apply numerical modeling to convert detrital muscovite $^{40}Ar/^{39}Ar$ thermochronology ages to erosion rates. In combination with detrital zircon U-Pb analysis, we aim to understand the spatio-temporal evolution of erosion and resultant exhumation, driving forces, and the relationship to crustal growth history in this region.

2. Geological setting

Our research area is located in the western part of the Himalaya and Tibetan Plateau (Fig. 1A), encompassing the Karakoram, Hindu Kush and Kohistan (Fig 1B). The Hindu Kush and Karakoram are part of the Asian plate and they formed an Andean-style margin prior to India-Asia collision (Hildebrand et al., 2000; Khan et al., 2009; Searle et al., 1987). The Cretaceous-Paleogene Kohistan Island arc (Searle et al., 1987; Treloar and Izatt, 1993) is sandwiched between the Indian and Asian plates (Fig. 1B). It is separated by the Main Karakoram Thrust (MKT) or Shyok Suture Zone (SSZ) from the Asian plate to the north, and by the Main Mantle Thrust (MMT) or the Indus Suture Zone (ISZ) from the Indian plate in the south (Fig. 1B).

Timing of collisions between the active margin of Asia (Karakoram, Hindu Kush and to the east the Lhasa terrane), India, and the Kohistan arc is debated. Whilst evidence has been provided both that the Kohistan Island Arc collided first with Asia prior to ~85–90 Ma (Searle et al., 1999; Searle et al., 1987; Treloar, 1997; Treloar and Izatt, 1993; Treloar et al., 1989) or with India at 65 or 50 Ma (Bouilhol et al., 2013; Khan et al., 2009), terminal suturing between India and Asia is considered by a majority of researchers to have taken place by 60–55 Ma (Hu et al., 2016 and references therein; Najman et al., 2017; Zhuang et al., 2015), although some have argued that it may have continued until circa 35 Ma or 25–20 Ma (Aitchison et al., 2007; Bouilhol et al., 2013; van Hinsbergen et al., 2012).

The Hindu Kush and Karakoram were Gondwana terranes in origin that drifted across the Tethys and collided with Asia during the Mesozoic Cimmerian orogeny (Angiolini et al., 2013; Faisal et al., 2014; Faisal et al., 2016; Şengör, 1984; Zanchi et al., 2000). The

Hindu Kush is considered to be the western continuation of the Wakhan Block — part of the South Pamir (Fig. 1B), both comprising an extended crust (Faisal et al., 2014; Zanchi et al., 2000). The Hindu Kush consists of deformed granitoids of Cambrian-Precambrian age, Paleozoic-Mesozoic metasedimentary successions, and Jurassic to mid-Cretaceous granitoids (Faisal et al., 2016; Zanchi et al., 2000). The Hindu Kush-South Pamir collided with the Central Pamir along the Rushan-Pshart suture zone around the Triassic-Jurassic boundary (Angiolini et al., 2013), as recorded by metamorphic monazite U-Pb ages of ca. 202–211 Ma (Faisal et al., 2014).

The Hindu Kush-South Pamir is separated from the Karakoram by the Wakhan-Tirich boundary zone (Fig. 1B). The two terranes were amalgamated in Early Jurassic times, as recorded by monazite U-Pb ages of ca. 185–190 Ma (Angiolini et al., 2013; Faisal et al., 2014; Zanchi and Gaetani, 2011). Following this crustal accretion event, an Andean-style subduction system was established to the south of the Asian margin comprised of Karakoram and Hindu Kush, as evidenced by, for example, the intrusion of the Karakoram Batholith dated at 95–130 Ma (e.g. Debon et al., 1987; Fraser et al., 2001; Heuberger et al., 2007) and the intrusion of plutons in the Hindu Kush at Tirich Mir dated at 127–123 Ma and Buni-Zom at 110–104 Ma (Faisal et al., 2016). Late Cretaceous monazites from Hindu Kush (Faisal et al., 2014) were interpreted to record regional metamorphism associated with the re-establishment of a subduction system farther to the south after the docking of Kohistan arc prior to 85–90 Ma (Fraser et al, 2001; Searle et al., 1999; Treloar et al., 1989).

The Karakoram terrane is broadly divided into three main units (Hildebrand et al., 2000; Searle et al., 1999), the Northern Karakoram Sedimentary Unit, the Southern Karakoram Metamorphic Belt, and the intervening Karakoram Batholith (Fig. 1B). The Northern Karakoram Sedimentary Unit consists of a mostly sedimentary belt which comprises pre-Ordovician crystalline basement covered by an Ordovician to Cretaceous sedimentary succession (Gaetani and Garzanti, 1991; Zanchi and Gaetani, 2011). The Karakoram Batholith includes pre-India-Asia collision, Andean-type, subduction-related granitoids (e.g. the Hunza Batholith) as above, and post-India-Asia collision leucogranites (e.g. the Baltoro Batholith) (Fig 1B). The Baltoro Plutonic Unit of the Karakoram Batholith was intruded between ca. 13 Ma and 25 Ma and represents post-India-Asia collision crustal thickening culminating in crustal melting (Parrish and Tirrul, 1989; Searle et al., 2010). Localized crustal melting and leucogranite intrusion in the Garam Chashma (Fig. 1B) area of Hindu Kush at ca. 22–29 Ma (Faisal et al., 2014; Faisal et al., 2016; Hildebrand et al., 1998) is contemporaneous with this event.

Metamorphism of the Southern Karakoram Metamorphic Belt spans from pre-India-Asia collision to Late Miocene but the record is spatially varied. Metamorphic ages as old as Late Cretaceous are documented in the Hunza region to the west, whilst along strike in the Baltoro region to the east no ages older than Late Oligocene are recorded (Palin et al 2012; Searle et al 2010). Regional metamorphism prior to India-Asia collision has been interpreted as due to the Asia-Kohistan Arc collision. Post-India-Asia crustal thickening and regional metamorphism is recorded in the Early Miocene in the Hunza region, approximately co-eval with crustal melting in the Baltoro region. The most recent phase of regional metamorphism occurred in the Late Miocene in the Baltoro region (Fraser et al 2001).

A disproportionate number of exhumation studies of the NW Himalayan region have focused on the Nanga Parbat syntaxis and the Karakoram Fault region (Boutonnet et al., 2012; Dunlap et al., 1998; Foster et al., 1994; Krol et al., 1996a; Mukherjee et al., 2012; Schärer et al., 1990; Schneider et al., 2001; Wallis et al., 2016; Zeitler et al., 2001). Rapid cooling associated with thrusting and strike-slip motion of the Karakoram Fault is constrained by $^{40}Ar/^{39}Ar$ (hornblende, muscovite, biotite, and K-feldspar) and apatite fission track dating to be around 13–17 Ma, 7–8 Ma and 3.3–7.4 Ma (Dunlap et al., 1998; Wallis et al., 2016). Contrasting with these young ages of rapid exhumation in the eastern Karakoram, Cretaceous/Paleocene-Eocene cooling ages (apatite and zircon fission track analysis and biotite K/Ar and Ar/Ar) have been reported in western Kohistan, East Hindu Kush, and the South Karakoram Metamorphic Belt (Treloar et al., 1989; Zeitler, 1985).

Whilst the majority of our study is focused on the Asian plate and Kohistan arc, our samples also cover a limited portion of the Indian plate south of the Main Mantle Thrust or Indus Suture zone (Fig. 1B). In the western Himalaya, the tectonostratigraphic zones that were identified in the central and eastern Himalaya (e.g. DeCelles et al., 2004), including Lesser, Higher, and Tethyan Himalayan zones, can be correlated to some extent, but they are not continuous with their correlatives to the west due to the lack of clear traces of major faults, such as the Main Central Thrust (DiPietro and Pogue, 2004). Unlike the main arc of the orogen, Neogene leucogranites are absent in the western Himalaya. Much of the metamorphism and deformation recorded in the west occurred in

Paleogene between 30 Ma and 50 Ma (Maluski and Matte, 1984; Smith et al., 1994; Treloar et al., 1989; Zeitler and Chamberlain, 1991).

3. Methodology

In order to obtain an overview of the geological evolution of the region, detrital muscovite $^{40}Ar/^{39}Ar$ thermochronological and detrital zircon U-Pb geochronological analyses were applied to six modern river sand samples draining the Hindu Kush, Karakoram and Kohistan Island Arc (Figs. 2 and 3; Table 1; Tables S1 and S2). Zircon U-Pb analyses were undertaken to study crustal accretion, muscovite $^{40}Ar/^{39}Ar$ analyses to study exhumation. We apply a multidimensional scaling (MDS) method for analyzing detrital zircon U-Pb data regarding provenance analysis (Fig. 4) and new MATLAB codes to implement the inversion of muscovite $^{40}Ar/^{39}Ar$ dates to erosion rates (Figs. 5 and 6; Table S3).

3.1. Modern river sediment samples

Six modern river sand (MRS) samples were taken from sidebars in channels of rivers that drain different terranes in the western Himalaya (Fig. 1). Two sub-samples were taken from one single bar and aggregated. Sample information including sampling coordinates is provided in Table 1. MRS 3 was taken from the Hunza River that drains a minor part of the Southern Karakoram Metamorphic Belt, the Karakoram Batholith and the Northern Karakoram Sedimentary Unit as well as the South Pamir in its upper headwaters. MRS 4 was collected from the Ghizar-Gilgit River that drains both the Karakoram (the Southern Karakoram Metamorphic Belt as well as Karakoram Batholith) and the Kohistan Island

Arc (Fig. 1A and 1B), MRS 2 (Gilgit River) was collected downstream of the confluence of the Hunza and Ghizar-Gilgit rivers (Fig. 1A and 1B).

MRS 5 was collected from the Chitral River that drains the Hindu Kush, the Karakoram (the Southern Karakoram Metamorphic Belt and Karakoram Batholith) and the Kohistan Island Arc. MRS 9 was taken from the Kabul River, which is the downstream continuation of the Chitral River, but at this location also flows over the Indian plate Himalaya. MRS 8 was taken from the Dir River that exclusively drain the southern part of Kohistan Island Arc (Fig. 1B).

3.2. Zircon U-Pb Analysis

Detrital zircon U-Pb ages for MRS 3, MRS 4, MRS 5, MRS 8, and MRS 9 were acquired using the London Geochronology Centre (LGC) facilities at University College London based on a New Wave 193 nm laser ablation system coupled to an Agilent 7700 quadrupole-based ICP-MS. Laser operating conditions for zircon used an energy density of ca 2.5 J/cm^2 and a repetition rate of 11 Hz. Repeated measurements of external zircon standard PLESOVIC (TIMS reference age 337.13±0.37 Ma) (Sláma et al., 2008) was used to correct for instrumental mass bias and depth-dependent inter-element fractionation of Pb, Th and U. Temora (Black et al., 2003) and 91500 (Wiedenbeck et al., 2004) zircons were used as secondary age standards.

Detrital zircon U-Pb ages for MRS 2 and an aliquot of MRS 3 were acquired using the Cameca IMS-1270 ion microprobe at Centre de Recherches Pétrographiques et Géochimiques (CRPG) at Nancy, France. Analytical procedures follow the method in

Deloule et al. (2002). Detrital zircon U-Pb ages for aliquots of MRS 3 from LGC and CRPG give the same range and the same dominant age components. Detrital zircon U-Pb ages are provided in supplementary materials (Table S1).

We will compare new detrital zircon U-Pb data collected on modern river sand samples (this study) from the Upper Indus tributaries with previous U-Pb data for the Indus River Mouth (Clift et al., 2004) and for the Upper Indus at Attock Bridge and various Himalaya tributaries (Alizai et al., 2011).

3.3. Muscovite $^{40}Ar/^{39}Ar$ Analysis

Optically pure (inclusion-free), sand-size grains of muscovite were hand picked. Muscovites were packed in aluminum foil, stacked in quartz tubes, shielded with Cd, and irradiated for 18 hours at the Oregon State University nuclear reactor. An in-house $^{40}Ar/^{39}Ar$ age standard, Drachenfels sanidine (DRA, 25.52 +/- 0.08 Ma) (Wijbrans et al., 1995), was used to monitor the neutron flux gradient. The analysis of single crystal muscovite follows the protocol in Sun et al. (2016). The program ArArCALC2.5 was used for data reduction and age calculations (Koppers, 2002). MRS 8 which was collected from the Dir River draining the Kohistan Island Arc only contains no muscovite. Detrital muscovite $^{40}Ar/^{39}Ar$ ages are provided in supplementary materials (Table S2).

3.4. Inversion of $^{40}Ar/^{39}Ar$ dates to erosion rates

Four methods for the inversion of detrital thermochronometer ages to erosion rates are summarized and contrasted in Table 2 (Table 2, Avdeev et al., 2011; Brandon et al., 1998; Brewer et al., 2003, 2006; Duvall et al., 2012; Garver et al., 1999; Ruhl and Hodges, 2005). The four methods share basic assumptions in numerical calculations: (1) they assume vertical trajectories without lateral variations through which particles are exhumed towards the surface; (2) the detrital minerals found in modern river sands are considered to be representative of the drainage; (3) the residence time of sediment-transport in the drainage basin is minimal; and (4) thermochronometric ages are the product of erosion rather than due to tectonic cooling or exhumation related to normal faulting. Two of these four methods were employed in this study, namely those of Avdeev et al. (2011) and Brandon et al. (1998).

The method developed by Avdeev et al (2011) allows temporal variation in erosion; whilst the other methods consider the time-averaged erosion rates (steady state) since the crystals passed through the closure isotherm. Avdeev et al. (2011) developed the approach by applying the Bayesian interpretation of probability and Markov Chain Monte Carlo algorithm in the inversion of detrital thermochronometer ages to erosion rates. The approach proposes age-elevation models with assumptions of a vertical advection path and a flat isotherm (Avdeev et al. 2011), which makes it suitable for thermochronometers with higher closure temperatures and its application to $^{40}Ar/^{39}Ar$ is highlighted in “future directions” in Avdeev et al. (2011). Avdeev's method allows investigation of temporal variation of erosion rates and has previously been applied to large drainages (e.g. the Yellow River, Yangtze, Mekong, etc.) of the central Tibetan Plateau with apatite U-Th/He and fission track analyses (Duvall et al., 2012). We developed a new MATLAB code according to Avdeev et al. (2011) and applied it to implement the Bayesian inversion of detrital muscovite $^{40}Ar/^{39}Ar$ dates (Fig. 5).

The method developed by Brandon et al. (1998) is founded on the different yield of detrital minerals of interest within the drainage basin and investigates the spatial variation in erosion. The different yield contrasts with the drainage-wide uniform assumption of the other three methods. Hence we explore this method as a complementary work to understand spatio-temporal evolution of erosion rates. Brandon et al. (1998) developed the approach by applying a simple one-dimensional analysis to convert detrital thermochronological ages to erosion rates. The approach has previously been applied to a modern river sand collected from the Indus river which had been previously analyzed by the zircon fission track technique (Garver et al., 1999). Later the approach has been expanded to include apatite and zircon U-Th/He, apatite and zircon fission track analysis, and $^{40}Ar/^{39}Ar$ thermochronometers (K-feldspar, biotite, muscovite, and hornblende) (Reiners and Brandon, 2006). We developed a new MATLAB code to conduct the inversion of detrital muscovite $^{40}Ar/^{39}Ar$ dates (Fig. 6) according to the methods in Brandon et al. (1998) and Willett and Brandon (2013).

We are interested in how erosion varies spatially across the region and within the same drainage basin, as well as how erosion might have evolved on long-time scales in response to the long-term accretion history of the region. Given the different focuses of the two methods and their match to our research interests, we apply Avdeev's method (Avdeev et al., 2011) with a focus on temporal evolution of erosion rates and Brandon's method (Brandon et al., 1998) with a focus on spatial variations to the inversion of detrital muscovite $^{40}Ar/^{39}Ar$ dates to erosion rates (Table S3). We use the two methods to invert thermochronometric ages to erosion rates and assume that the basic assumptions for numerical modeling are fulfilled. We further argue that because this region has long been in a contractile tectonic setting, we can ignore normal faulting related exhumation and cooling as a major control on mica cooling ages. For sample MRS 3, we observe that the distributions of mica thermochronometric ages and detrital zircon U-Pb geochronological ages show no overlap (Fig. 3A) and we take this as supportive evidence that thermochronometry ages reflect post-crystallization erosion-related cooling if white micas and zircons are derived from the same lithological units. We also consider the effects of transient adjustments to the thermal field driven by changes in rock uplift rates using two different approaches, namely those of Avdeev et al., (2011), Brandon et al. (1998) and Willets and Brandon (2013). We use results from both methods to investigate the variation in erosion of the drainage basin through space and time.

4. Results

4.1 Detrital zircon U-Pb ages

The detrital zircon U-Pb ages from modern river sediments of Indus tributaries (MRS 2, MRS 3, MRS 4, MRS 5, MRS 8, and MRS 9) are presented in Figures 2 and 3 along with compiled published bedrock data from the source terranes. Generally, young detrital zircon U-Pb ages (< 200 Ma) are predominant in samples of MRS 2, MRS 3, MRS 4, and MRS 8. MRS 2, MRS 3, and MRS 4 have similar age spectra (Fig. 3A, 3B, and 3C).

The U-Pb age spectrum of MRS 3 is characterized by peaks at ca. 50 Ma, 70 Ma, and 110 Ma with a few grains at ca. 80 Ma and 90 Ma. It lacks Neogene grains. The spectrum matches with the published compilation characteristic signature of the Karakoram and the South Pamir (Fig. 2A and 2B and Fig. 3A and 3G). The U-Pb age spectrum of MRS 4 is similar as that of MRS 3. It is dominated by age components of ~40–80 Ma and ~100–120 Ma with several grains around 80 Ma, 90 Ma, and 130 Ma. MRS 2 has a dominant age peak at 100–120 Ma with subordinate peaks at 40 Ma, 60 Ma, and 130 Ma (Fig. 3C). MRS 8 has a dominant age peak at ca. 40–60 Ma and some grains between 80 Ma and 100 Ma.

Samples MRS 5 and MRS 9 have substantial amounts of pre-Cambrian grains (Fig. 2A). For < 200 age components, the spectrum of MRS 5 shows peaks at ca. 60 Ma, 90 Ma, 110 Ma, and 200 Ma (Fig. 3E). MRS 9 has a similar spectrum to MRS 5 but with a broad distribution from ca. 30 Ma to 200 Ma (Fig. 3F).

In the multidimensional scaling plot (Fig. 4), samples MRS 2, MRS 3, and MRS 4 lie between the poles of the Karakoram, Hindu Kush, South Pamir, and Kohistan Island Arc. MRS 2 and MRS 3 are closer to the pole of the South Pamir. MRS 8 is the only sample close to the Kohistan Island Arc. MRS 5 and MRS 9 have an unexpected high input of Precambrian grains that results in an affinity close to the poles of terranes that are typified by such old grains in the MDS plot (Fig. 4), such as the Indian plate.

4.2 Detrital muscovite $^{40}Ar/^{39}Ar$ ages

4.2.1 $^{40}Ar/^{39}Ar$ ages

We have dated 356 detrital muscovite grains. All grains are younger than 200 Ma (most < 120 Ma), except one grain from MRS 3 that has an age of 267.8 Ma (Table S2).

Samples MRS 3 and MRS 4, despite being collected from rivers draining similar tectonic terranes (the Northern Kohistan Arc, the South Karakoram Metamorphic Belt and the Karakoram Batholith for MRS 4; minor part of the South Karakoram Metamorphic Belt, the Karakoram Batholith, the Northern Karakoram Sedimentary Unit and South Pamir for MRS 3), show distinct detrital muscovite $^{40}Ar/^{39}Ar$ age distributions (Fig. 3A and 3B). MRS 3 from the Hunza River has a range of $^{40}Ar/^{39}Ar$ ages between 4.4–32.3 Ma (most grains aged < 13 Ma, 60 out of 71 grains) (Fig. 3A), which is broadly consistent with a range of thermochronological techniques in bedrock data from that region (Krol et al 1996b). $^{40}Ar/^{39}Ar$ ages for the Ghizar-Gilgit River (MRS 4) range between 24.6 Ma and 102.5 Ma with peaks at ca. 30 Ma, 50 Ma, 70 Ma, and 100 Ma (Fig. 3B).

Muscovites are extremely rare in the igneous units of the Kohistan Island Arc (Parrish and Tirrul, 1989; Schärer et al., 1990; Searle et al., 1992) (e.g. MRS 8 with no micas collected from the Dir River which drains the Kohistan Island Arc only). We therefore interpret muscovites from MRS 4 as Karakoram-derived, including the South Karakoram Metamorphic Belt and the Karakoram Batholith. These white mica $^{40}Ar/^{39}Ar$ ages are consistent with bedrock hornblende, biotite, and muscovite ages reported by Treloar et al (1989) from the Karakoram in the region of this river's headwaters.

$^{40}Ar/^{39}Ar$ ages of micas from MRS 2 concentrate between 3.4 Ma and 39.8 Ma with a couple of grains at 70 Ma (Fig. 3C). MRS 2 is collected downstream of the confluence of Hunza River (MRS 3) and Ghizar-Gilgit River (MRS 4); its age spectrum overlaps and shares characteristics with MRS 3 and MRS 4 but loses the age peaks of 50 Ma and 100 Ma recorded in MRS 4 (Fig. 3B and 3C).

Most $^{40}Ar/^{39}Ar$ ages of MRS 5 collected from the Chitral River (draining the Hindu Kush and Karakoram, and a small proportion of the Kohistan Island Arc which does not contain muscovites) are between 110 Ma and 120 Ma with some grains around 20 Ma, 60 Ma, and 200 Ma (Fig. 3E). The downstream MRS 9, with a similar source catchment to MRS 5 with the addition of the Indian plate, has a similar range in $^{40}Ar/^{39}Ar$ age distribution (20-200 Ma) as MRS 5 but it has a major peak around 20 Ma (Fig. 3F).

4.2.2 Modeled erosion rates

We apply two newly developed MatLab codes to the inversion of detrital muscovite $^{40}Ar/^{39}Ar$ ages to erosion rates (Figs. 5 and 6). The method of Avdeev et al. (2011) focuses on temporal variations, allowing evaluation of erosion histories, whilst the method of Brandon et al. (1998) emphasizes the spatial variation in erosion in the drainage basin (Table 2).

4.2.2.1 Long-term erosion rate variations

Numerical modeling by using the method proposed by Avdeev et al. (2011) reveals temporal variations in erosion across the Hindu Kush-Karakoram. To the first order observation, the numerical modeling results using the method of Avdeev et al. (2011) reveal the most recent and greatest erosion in the Hunza River drainage (MRS 3) in the eastern Karakoram (Fig. 5). The erosion rate increases from 0.09 mm/yr to 0.60 mm/yr at ca. 8 Ma (Fig. 5C). MRS 4 from the Ghizar-Gilgit River, with muscovites interpreted as derived from the Karakoram since the Kohistan Island Arc contains only sparse muscovites, shows a relatively fast erosion rate of 0.19 mm/yr between ca. 35 Ma and ca. 25 Ma, and a rate of 0.29 mm/yr between 71 Ma and 69 Ma (Fig. 5F).

Numerical modeling results reveal that the Chitral drainage of MRS 5 experienced fast erosion (0.30 mm/yr) between ca. 115 Ma and ca. 124 Ma with slow erosion before and after this period (Fig. 5I; Table S3). Given the drainage basin from which this sample was collected, this most likely reflects erosion in the Hindu Kush and/or western Karakoram. The numerical modeling results for MRS 9 capture slow erosion prior to 129 Ma, which is followed by fast erosion (0.17mm/yr) between 125 Ma and 129 Ma, a protracted period of extremely slow erosion (< 0.09 mm/yr) since 125 Ma, and the fastest erosion (0.31 mm/yr) starting at ca. 27 Ma.

4.2.2.2 Spatially varying erosion rates

Numerical calculations using the method developed by Brandon et al. (1998) give temporally averaged but spatially varying erosion rates (Fig. 6). When plotting detrital ages, we choose the standard statistical technique of Kernel Density Estimation (KDE). As argued by Vermeesch (2012), the KDE serves as a robust alternative to the Probability Density Plot (PDP). In addition, the analytical errors are very low for Ar/Ar data (most are much less than 1%; Table S2) and hence error contributions to the variance of age measurements are negligible (Vermeesch, 2012) and are not considered in KDE and cumulative probability calculations. We hence choose the KDE to present individual detrital ages and modeled erosion rates and the cumulative probability for the erosion rate distribution with regard to drainage basin area (Fig. 6).

The first order observation reveals that 1) erosion rates are low for drainages of MRS 4 (micas derived from the Karakoram), MRS 5 (micas derived from the Hindu Kush and/or western Karakoram), and MRS 9 (downstream of MRS 5); 2) the Hunza River drainage of MRS 3 (micas derived from the eastern Karakoram and South Pamir) has the highest rates (Fig. 6). The erosion rate varies from < 1 mm/yr to > 2 mm/yr. The median value of 1.14 mm/yr (Fig. 6) suggests that more than half of the Hunza drainage of MRS 3 has an erosion rate > 1.14 mm/yr. Along with a narrow distribution of young $^{40}Ar/^{39}Ar$ ages, modeling results indicate young (< 8 Ma) and fast erosion in the Hunza River drainage. By contrast, the median erosion values for MRS 4, MRS 5, and MRS 9 are 0.15 mm/yr, 0.06 mm/yr, and 0.32 mm/yr, respectively (Fig. 6F, 6L, and 6O), indicating slow erosion in the Hindu Kush-Kohistan-western Karakoram.

5. Discussion

5.1 Characterization of source terranes with detrital zircon U-Pb geochronology

As expected (see Alizai et al., 2011), the spectra from the upper Indus tributaries are distinct from those rivers draining Indian plate Himalayan formations in their significant young < 200 Ma populations (Figs. 2 and 3); this reflects their drainage area encompassing the pre-collisional Andean-type subduction-related batholiths and the Kohistan Island Arc. The sample from the Indus River mouth has a hybrid spectrum (TH-1 in Fig. 2A) representing both young ages from the upper Indus tributaries and Paleozoic-Precambrian grains which are predominant in tributaries draining the Indian plate Himalaya (Fig. 2B) and in TH-1 (Fig. 2A).

The comparison with spectra of source terranes (Fig. 2B and Fig. 3G) and the MDS analysis of sample MRS 3 (Fig. 4) are consistent with the drainage basin geology in that the detritus is derived from the Karakoram and South Pamir. The lack of Cenozoic peak in MRS 3, typical of the Karakoram terrain from bedrock studies (Fig. 3A and 3G), is likely due to the fact that post-collisional Cenozoic plutons are volumetrically minor, and their prevalence has been over-enhanced in the published compilation spectrum due to the focus of published research on such rocks.

The greater affinity of MRS 3 and MRS 2 to the South Pamir compared to MRS 4 (Fig. 4) reflects the difference in drainage basins, with MRS 2 and 3, but not MRS 4, including the South Pamir in their catchment areas, and MRS 4 consisting of a higher percentage of Kohistan arc. This is consistent with the ~40–80 Ma peak dominant in MRS 4 which is strongly represented in MRS 8 (Dir River) (Fig. 3B, 3D, and 3G), which exclusively drains the Kohistan arc and shows strong affinity to the pole of Kohistan Island Arc on the multidimensional scaling plot (Fig. 4).

Prevalence of old, potentially recycled, grains in MRS 5 may be the result of this river's long transit through a zone of sedimentary rocks in the Tirich Mir fault-Wakhan Fault Zone. The 200 Ma peak and prevalence of older grains is also observed in MRS 9 (Fig. 3F). The Kabul River, from which MRS 9 was collected (Fig. 1A and 1B), drains the same terrains as MRS 5, with additional source downstream of Indian plate, contributing to the Precambrian zircons at the MRS 9 location. MRS 9's affinity to Asian contributions is supported by the similar detrital zircon U-Pb spectrum to that of the Upper Indus sediment sample collected at Attock (Fig. 2A); MRS 9 and the Attock sample cannot be differentiated on the multidimensional scaling plot (Fig. 4).

Hildebrand et al. (2001) noted that the 200 Ma population had been recorded in the Hindu Kush, but nowhere else along the southern margin of Asia. Our data would lend support to this observation in that the two samples which have a drainage area that includes the Hindu Kush (samples MRS 5 and MRS 9) contain grains of such an age, whilst the samples draining the Karakoram but not the Hindu Kush (samples MRS 2, MRS 3, and MRS 4) do not (Figs. 3A to 3C, 3E and 3F). Whilst it is conceivable that such a population in these two rivers was derived from the Kohistan Island Arc, rather than the Hindu Kush, we think this highly improbable since: 1) such grains are rare in Kohistan (samples MRS 2, MRS 4, MRS 8) (Fig. 3B to 3D); 2) samples MRS 5 and MRS 9 do not display the ~40–80 Ma peak characteristic of the Kohistan Island Arc (Fig. 3E and 3F), and 3) the Chitral-Kabul River's drainage basin only includes a small proportion of the Kohistan island arc (Fig. 1B).

The origin of the significant Paleogene population (30–37 Ma, peak at 35 Ma, plus a few grains at ca. 50 Ma) recorded in MRS 9 is enigmatic. The significance of the peak in the downstream MRS 9, and complete absence of a similar peak in the upstream MRS 5 might suggest that the grains come from the Indian plate, through which the river of the downstream sample only flowed. Whilst Paleogene granites have been recorded in the western part of the Indian plate, dated at 47 Ma from the Malakand granite (Smith et al., 1994) and 35 Ma from the leucogranite dikes in Swat, exposed in a nappe-scale duplex associated with southward directed thrusts (Lawrence et al., 1985; Zeitler and

Chamberlain, 1991), this region has been poorly mapped. Mineral cooling ages indicate that peak metamorphism occurred around 30–50 Ma (Maluski and Matte, 1984; Smith et al., 1994; Treloar et al., 1989), and thus zircons of such age may be documented with further work in the area. Nevertheless, if significant Indian plate input contributed to the zircon population, a concomitant increase in zircons of Precambrian and lowest Palaeozoic would be expected (Fig. 2A).

An alternative source for these Palaeogene zircons could be the Asian plate north of the arc. In this case, we would suggest that the lack of such a peak in MRS 5 is the result of increasing inputs of an unidentified source from the Asian plate to MRS 9 from Afghan tributaries with unstudied drainage basin geology, joining the Kabul River downstream of MRS 5. Grains of Palaeogene age have been recorded in the Kohistan arc (e.g. Bouilhol et al., 2013; Heuberger et al., 2007), yet two lines of evidence suggest that the Kohistan Island Arc is not the source of the grains in MRS 9: firstly, the Kohistan batholith only forms a minor part of this drainage basin for MRS 5 and MRS 9 (Fig. 1B); secondly, the appearance of these Palaeogene zircons in MRS 9 is accompanied by the significant appearance downstream of similar aged muscovites (Fig. 3F). Micas are absent from the Kohistan island arc.

With the level of bedrock characterization currently available, it is not possible to determine with any level of confidence from where these Paleogene grains were derived. Indeed, similar aged Paleogene zircons have been also reported in the Katawaz Basin and Makran accretionary wedge to the south and the southwest of our studied area (Fig.1A) and have similar levels of debated provenance; sediments in these two basins were argued to be derived either from the proto-Himalayan orogen (Carter et al., 2010) or from a local source of continental arc and ophiolites from the Makran (Mohammadi et al. (2016).

5.2 Long-term accretion histories and spatio-temporal evolution of erosion

5.2.1. Events related to the construction of the southern margin of Asian

The earliest recorded Mesozoic crustal accretion is documented by a population of ~200 Ma detrital zircon U-Pb ages (Figs. 3E and 3F) and co-eval rapid cooling, possibly captured by few detrital muscovite $^{40}Ar/^{39}Ar$ ages of ca. 180–196 Ma of MRS 5 and MRS 9 in the Hindu Kush. Hildebrand et al. (2001) noted that zircons of such age have not yet been recorded in the Karakoram, an observation which is upheld by our new data from the Karakoram-draining rivers (MRS 2, 3, and 4). Previous work records such ages in the Hindu Kush in monazites from metasedimentary rocks (Faisal et al., 2014; Hildebrand et al., 2001), located close to MRS 5. Faisal et al. (2014) record monazite populations dated at ca. 202–211 Ma and ca. 185–190 Ma, which they interpret as either reflecting a single protracted metamorphic event, or two events, related first to the collision of the Hindu Kush with the Central Pamir along the Rushan-Pshart Suture, and then to the collision of the Karakoram with the Hindu Kush along the Tirich Mir-Wakhan Fault zone. Detrital zircon U-Pb ages of ~200 Ma from MRS 5 and MRS 9, covering a period from ca. 191–212 Ma, overlap these two previously recorded age populations. We speculate that the presence of ca. 200 Ma population in the Hindu Kush (also recorded in the correlative South Pamir, e.g. Blayney et al 2016), but its lack of documentation, to date, in the Karakoram, may be the result of the docking of the Hindu Kush–South Pamir terrane with the Central Pamir at this time, closely followed by the closure of the basin between the Hindu Kush and Karakoram along the Tirich Mir-Wakhan Fault zone to the south (e.g. Faisal et al., 2014).

Zircons <200 Ma reflect the ongoing closure of Neotethys culminating in the eventual collision of India with Asia. All samples draining the Karakoram and Hindu Kush show a dominant peak of detrital zircon U-Pb ages at ca. 100–120 Ma (Fig. 3). This is consistent with previous work documenting similar zircon and monazite ages (95–130 Ma) in both terranes (e.g. Debon et al., 1987; Faisal et al., 2016; Fraser et al., 2001; Heuberger et al., 2007), which is related to the subduction of Neotethys beneath the southern margin of the Andean-style margin of Asia. Two phases of fast cooling/erosion at ca. 115–124 Ma and 125–129 Ma, modeled in the MRS 5 and MRS 9 of the Chitral and Kabul river samples, overlap in zircon and monazite ages and likely represent a single protracted event across the South Asian margin of the Hindu Kush/Karakoram, related to the same subduction system. Additional evidence of fast erosion in the Hindu Kush at this time comes from the Cretaceous Reshun conglomerate unit in the Tirich Mir fault zone; its existence implies that the Hindu Kush was acting as an active source during the deposition of this conglomerate (Pudsey et al., 1985). Early Cretaceous subduction and accretion processes are also widely observed in the Karakoram (e.g. Alizai et al., 2011; Hildebrand et al., 2001; Searle and Tirrul, 1991; Searle, 1991); U-Pb dating on the Hushe gneiss, Hunza granodiorite, and K2 gneiss constrain the subduction and accretion events to ca. 100–140 Ma. Subduction-related orogenic processes are supported by the presence of the synorogenic Tupop conglomerate unit which was deposited in the northern Karakoram (Gaetani et al., 1993). According to Faisal et al. (2014), subduction beneath the South

Asian margin of the Hindu Kush/Karakoram ceased in the Late Cretaceous due to collision of the Kohistan Island arc with the Asian margin at ~85–90 Ma. They interpret monazite ages of 88 and 72 Ma in the Hindu Kush as the result of the re-establishment of the subduction zone to the south. A scarcity of zircon ages in the range of ~80–90 Ma for all of our Hindu Kush- and Karakoram-draining samples may reflect this southerly jump in the location of subduction. The comparatively high erosion rate (~0.29 mm/yr) at 69–71 Ma from MRS 4 (Fig. 5) might reflect this collision-related erosion in the Southern Karakoram Metamorphic Belt.

5.2.2. Events related to the India-Asia collision.

Post-India-Asia collision fast erosion was modeled to occur at ca. 25–35 Ma in the Ghizar-Gilgit drainage in the western Karakoram (MRS 4) and at ca. 27 Ma in the Chitral-Kabul drainage in the Hindu Kush / western Karakoram (MRS 9). Additionally, MRS 5 has a small peak of detrital muscovite $^{40}Ar/^{39}Ar$ ages between ca. 18 Ma and 28 Ma (five grains; Table S3), possibly linked to fast erosion at this time in Chitral River drainage although the numerical modeling did not capture this signal due to the preponderance of ~120 Ma aged grains (Figs. 3 and 5).

In contrast to MRS 4's youngest record of fast erosion at 25–35 Ma (Fig 5, Table S3) and youngest mica age peak at 25–30 Ma respectively, MRS 3, along strike to the East, has a very different pattern of mica age distribution and erosion rates. MRS 3 displays the most recent intense erosion in all samples, as reflected in the concentration of young detrital muscovite $^{40}Ar/^{39}Ar$ ages (youngest age: 4.4 Ma; 61 out of 71 grains younger than 13 Ma,

Table S2; Fig. 3A), and the modeled fastest erosion rate (0.60 mm/yr at ca. 8 Ma) (Fig. 5C; Table S3).

We consider that the difference in mica ages and periods of rapid erosion between samples MRS 3 and 4, along-strike in the Karakoram may be the result of either: (1) proximity of MRS 3 river's headwaters to the Karakoram Fault, along which fast erosion of similar age has already been recorded at a number of locations (e.g. Dunlap et al., 1998; Wallis et al., 2016), or (2) along-strike variation in the tectonics of the Karakoram. This finding is consistent with previous basement rock thermochronology and thermal modeling studies in the western Kohistan and western Karakoram which reveal easterly decrease in biotite, zircon, and apatite cooling ages (Treloar et al., 1989; Zeiter et al., 1985), supporting our modeling with detrital muscovite. Both Searle et al (2010) and Palin et al (2012) noted differences between the western (Hunza) and eastern (Baltoro) regions in terms of their metamorphic and magmatic histories. They ascribed this difference to either diachroneity of evolution along strike in the Karakoram, or variation in the degree of exhumation. Modelling results on MRS 3 from the Hunza River indicate that the Late Miocene rapid exhumation experienced in the Baltoro Region of the Karakoram (Cerveny et al., 1989; Foster et al., 1994) extends at least as far west as the eastern part of Hunza Pluton, consistent with the work of Krol et al (1996b).

Wallis et al. (2016) identified a northward increase in erosion rate across the Indus suture zone from the Ladakh Island Arc to the Karakoram (Fig. 7A). They proposed a driving force related to the gradient in the crustal shortening and thickening driving the uplift and causing variations in erosion which is focused in the Karakoram. In our study, the modeling on samples MRS 3 and MRS 4 which were collected from different parts of Karakoram indicates that a similar northward increase in erosion rate was recorded as far west as the Hunza River, if the locus of our recorded rapid erosion in the Hunza River sample MRS 3 is taken to be the Karakoram Batholith rather than the region of the Karakoram Fault in the river's headwaters. It should be noted that in this study erosion rate increases from the Southern Karakoram Metamorphic Belt which the Ghizar-Gilgit River mainly drains (MRS 4) to the Karakoram Batholith and Northern Karakoram Sedimentary Unit where the Hunza River drains (MRS 3), unlike the eastern Karakoram where the erosion rate increases across the Indus suture (Wallis et al., 2016). No evidence of Neogene fast erosion or northward increase in erosion rate is recorded still further west, as the remaining part of our study area (Hindu Kush, Kohistan, and the western Karakoram) are characterized by both pre- and post-India-Asia fast erosion older than ca. 25 Ma (Fig. 7A).

The modeled late Miocene fast erosion of MRS 3, along with previous studies (Fig. 7A), indicates that a region extending from the Hunza River drainage (including the easternmost Hunza Pluton) to the easternmost Karakoram experienced rapid exhumation. Modeled fast erosion since ca. 8 Ma in central Karakoram is consistent with deeply eroded and exposed deep crustal materials (Searle, 2015). What is most striking is the consistency between the reconstructed erosion histories (east-west variations with fast erosion focusing on the east-central Karakoram) and the topographic profile across the region of the Hindu Kush-Kohistan-Karakoram. Generally, the entire region is high but the east-central Karakoram has higher elevation (5 to 6 km versus 4 to 5 km in the western Karakoram-Hindu Kush-Kohistan) and greater relief (Fig. 7B). Seismic studies show that the crustal thickness increases from less than 50–60 km in the Hindu Kush-Kohistan in the west and Tethyan Himalaya in the south to approximately 80 km in the central Karakoram fault zone (e.g. Hazarika et al., 2014; Holt and Wallace, 1990; Rai et al., 2006; Wittlinger et al., 2004); this difference in crustal thickness reflects more intense crustal shortening in the east-central Karakoram since the late Miocene compared to surrounding areas (Searle et al., 2010). We suggest that the consistent patterns of greater erosion, topography, and crustal thickness in the east compared to the west of the Karakoram suggest a genetic relation; the recent (since ca. 8 Ma) intense crustal shortening and thickening in the east-central Karakoram drove the uplift, raising the elevation, which in turn promoted the erosion (hence exhumation) and generation of extreme relief, resulting in the topographic difference between two regions identified in this study (Fig. 7B).

The modeled fast erosion in the east-central Karakoram since ca. 8 Ma is consistent with the foreland basin record. Chirouze et al. (2015) conducted a study of bulk trace element and Hf-Nd isotopes, and detrital zircon fission track analyses on modern Indus and paleo-Indus deposits in the western Himalayan foreland. Their results indicate increasing contribution of inputs from the Karakoram to the late Miocene Siwalik sediments, consistent with our documentation of fast erosion with modeling of detrital muscovite $^{40}Ar/^{39}Ar$ ages.

6. Conclusions

New zircon and mica data and modeled erosion rates add to a growing dataset aiding our understanding of spatial and temporal accretion histories and impacts in the western

Himalaya-south Asian margin. Our study supports contributions of polyphase collisions and associated crustal accretion, shortening, and thickening to the construction of present-day high topography in the region of Hindu Kush-Kohistan-Karakoram. This process started with the Mesozoic amalgamation of the various Gondwanan terranes. Our data from this region show a) further support to the suggestion that the ca. 200 Ma detrital zircon population present in the Hindu Kush is absent from the Karakoram, and may reflect the collision between the Hindu Kush-South Pamir with Central Pamir, b) a dominant arc-derived peak of detrital zircon U-Pb ages at ca. 120 Ma in all MRS samples, and c) fast erosion pre-India-Asia collision at 115–129 Ma and 69–71 Ma. The India-Asia collision is the most influential factor affecting erosion rate, as evidenced by pervasive post-collision fast erosion periods recorded at 35 Ma, 27 Ma and 8.5 Ma. There is also significant spatial variation in erosion, in particular the rapid erosion at 8 Ma is only observed farthest east in our study area. Such a variation may reflect influence of the Karakoram Fault and/or east-west along-strike variations in crustal shortening and thickening and associated uplift.

Acknowledgements

We would like to thank Kyle Larson, Mathieu Soret, an anonymous reviewer, and the editor Ian Fitzsimons for their critical reviews that greatly improved this paper. Financial support was provided under the Initial Training Network iTECC by the EU REA under the FP7 implementation of the Marie Curie Action (grant # 316966). We thank Xiaobin Cao and Mark Brandon for discussions on the interpretation of detrital thermochronometric dates. Etienne Deloule, Michel Champenois, Gwladys Govin, and

Jesse Davenport are acknowledged for help during detrital zircon U-Pb analysis at CRPG (CNRS).

Figure Captions

Figure 1. (A) Shaded relief map (Amante, 2009) of western Himalaya and Tibetan Plateau with major geological features and Indus and Ganges drainages and their boundary (dotted line). Collection sites of modern river sediment samples (MRS 2, 3, 4, 5, 8, and 9, this study) are indicated by blue solid circles. Purple (white) solid circles indicate previous sampling sites of Himalaya tributary river sediments (a–g) (Alizai et al., 2011), and modern river sediments at the Indus River mouth (TH-1) (Clift et al., 2004)**.** **(B)** Simplified geology, showing the major terranes and their sub-divisions, along the Upper Indus with tributaries and sample locations of modern river sediment (MRS) samples. Main Karakoram Thrust (MKT) / Shyok Suture Zone (SSZ), Main Mantle Thrust (MMT) / Indus Suture Zone (ISZ).

Figure 2. (A) Detrital zircon U-Pb age cumulative curves of modern river sediments of the Upper Indus tributaries (MRS 2, 3, 4, 5, 8, and 9; this study), Indus River mouth sample TH-1 (Clift et al., 2004), and the Upper Indus at Attock Bridge and Himalayan tributaries (Alizai et al., 2011). **(B)** Probability density curves of detrital zircon U-Pb dates of potential source terranes. Data are compiled from previous publications for Kohistan-Ladakh oceanic arcs (Bosch et al., 2011; Bouilhol et al., 2011, 2013; Clift and Gaedicke, 2002; Henderson et al., 2011; Heuberger et al., 2007; Honegger et al., 1982; Jagoutz et al., 2009; Khan et al., 2009; Krol et al., 1996a; Ravikant et al., 2009; Schärer et al., 1984; Singh et al., 2007; St-Onge et al., 2010; Upadhyay et al., 2008; Weinberg et

al., 2000; White et al., 2011), Karakoram (Fraser et al., 2001; Heuberger et al., 2007; Jain and Singh, 2008; Mahar et al., 2014; Parrish and Tirrul, 1989; Phillips et al., 2004; Ravikant et al., 2009; Schärer et al., 1990; Searle et al., 1998; Sen et al., 2014; Weinberg et al., 2000), Hindu Kush (Hildebrand et al., 1998; Hildebrand et al., 2001), and South Pamir (Blayney et al., 2016). Detrital zircon U-Pb ages for terrains of Tethyan Himalaya, Lesser Himalaya, and Higher Himalaya are compiled from Clift et al., (2014), Gehrels et al. (2003, 2008), and Hu et al. (2010).

Figure 3. (A-F) Histograms of detrital muscovite $^{40}Ar/^{39}Ar$ ages and detrital zircon U-Pb ages (0~240 Ma). Note the Dir River where MRS 8 was collected drains the Kohistan arc exclusively and MRS 8 has no muscovites. **(G)** Kernel Density Estimation (KDE) (Vermeesch, 2012) plot of compiled detrital zircon U-Pb ages of potential source terranes. For cited references of potential source terranes, refer to Figure 2 caption.

Figure 4. A multidimensional scaling plot (Vermeesch, 2013) of detrital zircon U-Pb ages displays the similarities/dissimilarities between the modern river sediment samples (MRS 2, 3, 4, 5, 8, and 9, this study; Upper Indus at the Attock Bridge and Himalaya tributaries, Alizai et al., 2011; lower Indus TH1, Clift et al., 2004) and potential source terranes (Lesser Himalaya–LH, Higher Himalaya–HH, Tethyan Himalaya–TH; Asian margin, including Karakoram–KK, Hindu-Kush–HK, and South Pamir–SP; Kohistan Island Arc–KLA). For cited references for potential source terranes, refer to Figure 2 caption.

Figure 5. Model results of MRS samples, obtained by applying new MATLAB code to implement Avdeev method (Avdeev et al., 2011) allowing variations in erosion rate

through time (discrete segments in elevation versus age profiles). **(Left column; A, D, G, J)** Plots of detrital muscovite $^{40}Ar/^{39}Ar$ age (Ma) against elevation (km). Dashed (black) line represents the best (average) model. **(Middle column; B, E, H, K)** Cumulative probability density plots showing actual ages (open circles) and synthetic ages modeled from the best model (dashed line) and the average model (solid line). **(Right column; C, F, I, L)** Plots of erosion rate versus time (Ma).

Figure 6. Model results obtained by applying the method of Brandon et al. (1998). **(Left column; A, D, G, J, M)** Kernel Density Estimation (KDE) (Vermeesch, 2012) and histogram plots of detrital muscovite $^{40}Ar/^{39}Ar$ age (Ma). **(Middle column; B, E, H, K, N)** Kernel Density Estimation (KDE) (Vermeesch, 2012) and histogram plots of modeled erosion rates. **(Right column; C, F, I, L, O)** Cumulative plot of modeled erosion rates shown with the median value.

Figure 7. (A) Studies highlight the east-west variation in erosional history. Line YZ indicates the topographic transect shown in **(B)**. Refer to Fig. 1B for cited references regarding previous studies.

Table 1. Sample collection site coordinates, drainage, and tectonic terranes.

Table 2. Comparison of methods for the inversion of detrital thermochronometer ages to erosion rates.

Cited References

1. Aitchison, J.C., Ali, J.R., Davis, A.M., 2007. When and where did India and Asia collide? Journal of Geophysical Research: doi:10.1029/2006JB004706.
2. Alizai, A., Carter, A., Clift, P.D., VanLaningham, S., Williams, J.C., Kumar, R., 2011. Sediment provenance, reworking and transport processes in the Indus River by U–Pb dating of detrital zircon grains. Global and Planetary Change 76, 33-55.
3. Amante, C., 2009. ETOPO1 1 arc-minute global relief model: procedures, data sources and analysis. http://www. ngdc. noaa. gov/mgg/global/global. html.
4. Angiolini, L., Zanchi, A., Zanchetta, S., Nicora, A., Vezzoli, G., 2013. The Cimmerian geopuzzle: new data from South Pamir. Terra Nova 25, 352-360.
5. Avdeev, B., Niemi, N.A., Clark, M.K., 2011. Doing more with less: Bayesian estimation of erosion models with detrital thermochronometric data. Earth and Planetary Science Letters 305, 385-395.
6. Black, L.P., Kamo, S.L., Allen, C.M., Aleinikoff, J.N., Davis, D.W., Korsch, R.J., Foudoulis, C., 2003. TEMORA 1: a new zircon standard for Phanerozoic U–Pb geochronology. Chemical Geology 200, 155-170.
7. Blayney, T., Najman, Y., Dupont-Nivet, G., Carter, A., Miller, I., Garzanti, E., Sobel, E.R., Rittner, M., Ando, S., Guo, Z., 2016. Indentation of the Pamirs with respect to the northern margin of Tibet: constraints from the Tarim Basin sedimentary record. Tectonics, 35, 2345–2369, doi:10.1002/2016TC004222.
8. Bosch, D., Garrido, C.J., Bruguier, O., Dhuime, B., Bodinier, J.-L., Padròn-Navarta, J.A., Galland, B., 2011. Building an island-arc crustal section: Time constraints from a LA-ICP-MS zircon study. Earth and Planetary Science Letters 309, 268-279.

9. Boutonnet, E., Leloup, P., Arnaud, N., Paquette, J.L., Davis, W., Hattori, K., 2012. Synkinematic magmatism, heterogeneous deformation, and progressive strain localization in a strike-slip shear zone: The case of the right-lateral Karakorum fault. Tectonics 31, 10.1029/2011TC003049.

10. Bouilhol, P., Jagoutz, O., Hanchar, J.M., Dudas, F.O., 2013. Dating the India–Eurasia collision through arc magmatic records. Earth and Planetary Science Letters 366, 163-175.

11. Bouilhol, P., Schaltegger, U., Chiaradia, M., Ovtcharova, M., Stracke, A., Burg, J.-P., Dawood, H., 2011. Timing of juvenile arc crust formation and evolution in the Sapat Complex (Kohistan–Pakistan). Chemical Geology 280, 243-256.

12. Brandon, M.T., Roden-Tice, M.K., Garver, J.I., 1998. Late Cenozoic exhumation of the Cascadia accretionary wedge in the Olympic Mountains, northwest Washington State. Geological Society of America Bulletin 110, 985-1009.

13. Braun, J., Van Der Beek, P., Batt, G., 2006. Quantitative thermochronology: numerical methods for the interpretation of thermochronological data. Cambridge University Press.

14. Brewer, I., Burbank, D., Hodges, K., 2003. Modelling detrital cooling-age populations: Insights from two Himalayan catchments. Basin Research 15, 305-320.

15. Brewer, I., Burbank, D., Hodges, K., 2006. Downstream development of a detrital cooling-age signal: Insights from $^{40}Ar/^{39}Ar$ muscovite thermochronology in the Nepalese Himalaya. Geological Society of America Special Papers 398, 321-338.

16. Burchfiel, B., Quidong, D., Molnar, P., Royden, L., Yipeng, W., Peizhen, Z., Weiqi, Z., 1989. Intracrustal detachment within zones of continental deformation. Geology 17, 748-752.

17. Carter, A., Najman, Y., Bahroudi, A., Bown, P., Garzanti, E., Lawrence, R.D., 2010. Locating earliest records of orogenesis in western Himalaya: Evidence from Paleogene sediments in the Iranian Makran region and Pakistan Katawaz basin. Geology 38, 807-810.

18. Cerveny, P.F., Naeser, C.W., Kelemen, P.B., Lieberman, J.E., Zeitler, P.K., 1989. Zircon fission-track ages from the Gasherbrum Diorite, Karakoram Range, northern Pakistan. Geology 17, 1044-1048.

19. Chirouze, F., Huyghe, P., Chauvel, C., van der Beek, P., Bernet, M., Mugnier, J.-L., 2015. Stable Drainage Pattern and Variable Exhumation in the Western Himalaya since the Middle Miocene. The Journal of Geology 123, 1-20.

20. Clift, P.D., Blusztajn, J., 2005. Reorganization of the western Himalayan river system after five million years ago. Nature 438, 1001-1003.

21. Clift, P.D., Campbell, I.H., Pringle, M.S., Carter, A., Zhang, X., Hodges, K.V., Khan, A.A., Allen, C.M., 2004. Thermochronology of the modern Indus River bedload: New insight into the controls on the marine stratigraphic record. Tectonics 23 doi:10.1029/2003TC001559.

22. Clift, P.D., Carter, A., Jonell, T.N., 2014. U–Pb dating of detrital zircon grains in the Paleocene Stumpata Formation, Tethyan Himalaya, Zanskar, India. Journal of Asian Earth Sciences 82, 80-89.

23. Clift, P.D., Gaedicke, C., 2002. Accelerated mass flux to the Arabian Sea during the middle to late Miocene. Geology 30, 207-210.

24. Debon, F., Le Fort, P., Dautel, D., Sonet, J., Zimmermann, J., 1987. Granites of western Karakorum and northern Kohistan (Pakistan): a composite Mid-Cretaceous to upper Cenozoic magmatism. Lithos 20, 19-40.

25. DeCelles, P., Gehrels, G., Najman, Y., Martin, A., Carter, A., Garzanti, E., 2004. Detrital geochronology and geochemistry of Cretaceous–Early Miocene strata of Nepal: implications for timing and diachroneity of initial Himalayan orogenesis. Earth and Planetary Science Letters 227, 313-330.

26. Deloule, E., Alexandrov, P., Cheilletz, A., Laumonier, B., Barbey, P., 2002. In-situ U-Pb zircon ages for Early Ordovician magmatism in the eastern Pyrenees, France: the Canigou orthogneisses. International Journal of Earth Sciences 91, 398-405.

27. DiPietro, J.A., Pogue, K.R., 2004. Tectonostratigraphic subdivisions of the Himalaya: A view from the west. Tectonics 23, DOI: 10.1029/2003TC001554.

28. Dunlap, W.J., Weinberg, R.F., Searle, M.P., 1998. Karakoram fault zone rocks cool in two phases. Journal of the Geological Society 155, 903-912.

29. Duvall, A.R., Clark, M.K., Avdeev, B., Farley, K.A., Chen, Z., 2012. Widespread late Cenozoic increase in erosion rates across the interior of eastern Tibet constrained by detrital low-temperature thermochronometry. Tectonics 31 doi:10.1029/2011TC002969.

30. Faisal, S., Larson, K.P., Cottle, J.M., Lamming, J., 2014. Building the Hindu Kush: Monazite Records of Terrane Accretion, Plutonism, and the Evolution of the Himalaya–Karakoram–Tibet Orogen. Terra Nova 26, 395-401.

31. Faisal, S., Larson, K.P., King, J., Cottle, J.M., 2016. Rifting, subduction and collisional records from pluton petrogenesis and geochronology in the Hindu Kush, NW Pakistan. Gondwana Research 35, 286-304.

32. Foster, D.A., Gleadow, A.J., Mortimer, G., 1994. Rapid Pliocene exhumation in the Karakoram (Pakistan), revealed by fission-track thermochronology of the K2 gneiss. Geology 22, 19-22.

33. Fraser, J.E., Searle, M.P., Parrish, R.R., Noble, S.R., 2001. Chronology of deformation, metamorphism, and magmatism in the southern Karakoram Mountains. Geological Society of America Bulletin 113, 1443-1455.

34. Gaetani, M., Garzanti, E., 1991. Multicyclic history of the Northern India continental margin (Northwestern Himalaya) (1). AAPG Bulletin 75, 1427-1446.

35. Gaetani, M., Jadoul, F., Erba, E., Garzanti, E., 1993. Jurassic and Cretaceous orogenic events in the North Karakoram: age constraints from sedimentary rocks. Geological Society, London, Special Publications 74, 39-52.

36. Garver, J.I., Brandon, M.T., Roden-Tice, M., Kamp, P.J., 1999. Exhumation history of orogenic highlands determined by detrital fission-track thermochronology. Geological Society, London, Special Publications 154, 283-304.

37. Gehrels, G., DeCelles, P., Martin, A., Ojha, T., Pinhassi, G., Upreti, B., 2003. Initiation of the Himalayan orogen as an early Paleozoic thin-skinned thrust belt. GSA today 13, 4-9.

38. Gehrels, G.E., Valencia, V.A., Ruiz, J., 2008. Enhanced precision, accuracy, efficiency, and spatial resolution of U-Pb ages by laser ablation–multicollector–inductively coupled plasma–mass spectrometry. Geochemistry, Geophysics, Geosystems 9, Q03017, doi:10.1029/2007GC001805.

39. Hazarika, D., Sen, K., Kumar, N., 2014. Characterizing the intracrustal low velocity zone beneath northwest India–Asia collision zone. Geophysical Journal International 199, 1338-1353.

40. Henderson, A.L., Najman, Y., Parrish, R., Mark, D.F., Foster, G.L., 2011. Constraints to the timing of India–Eurasia collision; a re-evaluation of evidence from the Indus Basin sedimentary rocks of the Indus–Tsangpo Suture Zone, Ladakh, India. Earth-Science Reviews 106, 265-292.

41. Heuberger, S., Schaltegger, U., Burg, J.-P., Villa, I.M., Frank, M., Dawood, H., Hussain, S., Zanchi, A., 2007. Age and isotopic constraints on magmatism along the Karakoram-Kohistan Suture Zone, NW Pakistan: Evidence for subduction and continued convergence after India-Asia collision. Swiss Journal of Geosciences 100, 85-107.

42. Hildebrand, P., Noble, S., Searle, M., Parrish, R., 1998. Tectonic significance of 24 Ma crustal melting in the eastern Hindu Kush, Pakistan. Geology 26, 871-874.

43. Hildebrand, P., Noble, S., Searle, M., Waters, D., Parrish, R., 2001. Old origin for an active mountain range: Geology and geochronology of the eastern Hindu Kush, Pakistan. Geological Society of America Bulletin 113, 625-639.

44. Hildebrand, P., Searle, M., Khan, Z., Van Heijst, H., 2000. Geological evolution of the Hindu Kush, NW Frontier Pakistan: active margin to continent-continent collision zone. Geological Society, London, Special Publications 170, 277-293.

45. Holt, W.E., Wallace, T.C., 1990. Crustal thickness and upper mantle velocities in the Tibetan Plateau region from the inversion of regional Pnl waveforms: Evidence for a thick upper mantle lid beneath southern Tibet. Journal of Geophysical Research: Solid Earth 95, 12499-12525.

46. Honegger, K., Dietrich, V., Frank, W., Gansser, A., Thöni, M., Trommsdorff, V., 1982. Magmatism and metamorphism in the Ladakh Himalayas (the Indus-Tsangpo suture zone). Earth and Planetary Science Letters 60, 253-292.

47. Hu, X., Garzanti, E., Wang, J., Huang, W., An, W., Webb, A., 2016. The timing of India-Asia collision onset–Facts, theories, controversies. Earth-Science Reviews 160, 264-299.

48. Hu, X., Jansa, L., Chen, L., Griffin, W.L., O'Reilly, S.Y., Wang, J., 2010. Provenance of Lower Cretaceous Wölong volcaniclastics in the Tibetan Tethyan Himalaya: Implications for the final breakup of eastern Gondwana. Sedimentary Geology 223, 193-205.

49. Jagoutz, O.E., Burg, J.-P., Hussain, S., Dawood, H., Pettke, T., Iizuka, T., Maruyama, S., 2009. Construction of the granitoid crust of an island arc part I:

geochronological and geochemical constraints from the plutonic Kohistan (NW Pakistan). Contributions to Mineralogy and Petrology 158, 739-755.

50. Jain, A.K., Singh, S., 2008. Tectonics of the southern Asian Plate margin along the Karakoram Shear Zone: Constraints from field observations and U–Pb SHRIMP ages. Tectonophysics 451, 186-205.

51. Khan, S.D., Walker, D.J., Hall, S.A., Burke, K.C., Shah, M.T., Stockli, L., 2009. Did the Kohistan-Ladakh island arc collide first with India? Geological Society of America Bulletin 121, 366-384.

52. Koppers, A.A., 2002. ArArCALC—software for ^{40}Ar/^{39} Ar age calculations. Computers & Geosciences 28, 605-619.

53. Krol, M.A., Zeitler, P.K., Copeland, P., 1996a. Episodic unroofing of the Kohistan Batholith, Pakistan: Implications from K-feldspar thermochronology. Journal of Geophysical Research: Solid Earth (1978–2012) 101, 28149-28164.

54. Krol, M.A., Zeitler, P.K., Poupeau, G., Pecher, A., 1996b. Temporal variations in the cooling and denudation history of the Hunza plutonic complex, Karakoram Batholith, revealed by ^{40}Ar/^{39}Ar thermochronology. Tectonics 15, 403-415.

55. Lawrence, R., Snee, L., Rosenberg, P., 1985. Nappe structure in a crustal scale duplex in Swat, Pakistan. Geol. Soc. Am., Abstr. Programs;(United States) 17.

56. Mahar, M.A., Mahéo, G., Goodell, P.C., Pavlis, T.L., 2014. Age and origin of post collision Baltoro granites, south Karakoram, North Pakistan: Insights from in-situ U–Pb, Hf and oxygen isotopic record of zircons. Lithos 205, 341-358.

57. Maluski, H., Matte, P., 1984. Ages of alpine tectonometamorphic events in the northwestern Himalaya (northern Pakistan) by 39Ar/40Ar method. Tectonics 3, 1-18.

58. McDougall, I., Harrison, T.M., 1999. Geochronology and Thermochronology by the ^{40}Ar/^{39}Ar Method. Oxford University Press.

59. Mohammadi, A., Burg, J.-P., Winkler, W., Ruh, J., von Quadt, A., 2016. Detrital zircon and provenance analysis of Late Cretaceous− Miocene onshore Iranian Makran strata: Implications for the tectonic setting. Geological Society of America Bulletin, v. 128, p. 1481–1499, doi: 10.1130/B31361.1.

60. Molnar, P., Tapponnier, P., 1975. Cenozoic tectonics of Asia: effects of a continental collision. Science 189, 419-426.

61. Mukherjee, B.K., Sen, K., Sachan, H.K., Paul, S.K., 2012. Exhumation history of the Karakoram fault zone mylonites: New constraints from microstructures, fluid inclusions, and 40 Ar-39 Ar analyses. Lithosphere 4, 230-241.

62. Najman, Y., Bickle, M., BouDagher-Fadel, M., Carter, A., Garzanti, E., Paul, M., Wijbrans, J., Willett, E., Oliver, G., Parrish, R., 2008. The Paleogene record of Himalayan erosion: Bengal Basin, Bangladesh. Earth and Planetary Science Letters 273, 1-14.

63. Najman, Y., Jenks, D., Godin, L., Boudagher-Fadel, M., Millar, I., Garzanti, E., Horstwood, M., Bracciali, L., 2017. The Tethyan Himalayan detrital record shows that India–Asia terminal collision occurred by 54 Ma in the Western Himalaya. Earth and Planetary Science Letters 459, 301-310.

64. Palin, R., Searle, M., Waters, D., Horstwood, M., Parrish, R., 2012. Combined thermobarometry and geochronology of peraluminous metapelites from the Karakoram metamorphic complex, North Pakistan; New insight into the tectonothermal evolution of the Baltoro and Hunza Valley regions. Journal of Metamorphic Geology 30, 793-820.

65. Parrish, R.R., Tirrul, R., 1989. U-Pb age of the Baltoro granite, northwest Himalaya, and implications for monazite U-Pb systematics. Geology 17, 1076-1079.

66. Phillips, R.J., Parrish, R.R., Searle, M.P., 2004. Age constraints on ductile deformation and long-term slip rates along the Karakoram fault zone, Ladakh. Earth and Planetary Science Letters 226, 305-319.

67. Pudsey, C., Coward, M., Luff, I., Shackleton, R., Windley, B., Jan, M., 1985. Collision zone between the Kohistan arc and the Asian plate in NW Pakistan. Transactions of the Royal Society of Edinburgh: Earth Sciences 76, 463-479.

68. Qasim, M., Ding, L., Khan, M.A., Umar, M., Jadoon, I.A., Haneef, M., Baral, U., Cai, F., Shah, A., Yao, W., 2017. Late Neoproterozoic–Early Palaeozoic stratigraphic succession, Western Himalaya, North Pakistan: Detrital zircon provenance and tectonic implications. Geological Journal 2017,1-22. DOI: 10.1002/gj.3063.

69. Rai, S., Priestley, K., Gaur, V., Mitra, S., Singh, M., Searle, M., 2006. Configuration of the Indian Moho beneath the NW Himalaya and Ladakh. Geophysical Research Letters 33.

70. Ravikant, V., Wu, F.-Y., Ji, W.-Q., 2009. Zircon U–Pb and Hf isotopic constraints on petrogenesis of the Cretaceous–Tertiary granites in eastern Karakoram and Ladakh, India. Lithos 110, 153-166.

71. Reiners, P.W., Brandon, M.T., 2006. Using thermochronology to understand orogenic erosion. Annu. Rev. Earth Planet. Sci. 34, 419-466.

72. Robinson, A.C., 2015. Mesozoic tectonics of the Gondwanan terranes of the Pamir plateau. Journal of Asian Earth Sciences 102, 170-179.

73. Ruhl, K., Hodges, K., 2005. The use of detrital mineral cooling ages to evaluate steady state assumptions in active orogens: An example from the central Nepalese Himalaya. Tectonics 24, TC4015, doi:10.1029/2004TC001712.

74. Schärer, U., Copeland, P., Harrison, T.M., Searle, M.P., 1990. Age, cooling history, and origin of post-collisional leucogranites in the Karakoram Batholith; a multi-system isotope study. The Journal of Geology, 233-251.

75. Schärer, U., Hamet, J., Allègre, C.J., 1984. The Transhimalaya (Gangdese) plutonism in the Ladakh region: a U Pb and Rb Sr study. Earth and Planetary Science Letters 67, 327-339.

76. Schneider, D., Zeitler, P., Kidd, W., Edwards, M., 2001. Geochronologic constraints on the tectonic evolution and exhumation of Nanga Parbat, western Himalaya syntaxis, revisited. The Journal of Geology 109, 563-583.

77. Searle, M., Crawford, M., Rex, A., 1992. Field relations, geochemistry, origin and emplacement of the Baltoro granite, central Karakoram. Transactions of the Royal Society of Edinburgh: Earth Sciences 83, 519-538.

78. Searle, M.P., 2015. Mountain building, tectonic evolution, rheology and crustal flow in the Himalaya, Karakorum and Tibet. Treatise on Geophysics 6, 469-511.

79. Searle, M.P., Khan, M.A., Fraser, J., Gough, S., Jan, M.Q., 1999. The tectonic evolution of the Kohistan-Karakoram collision belt along the Karakoram Highway transect, north Pakistan. Tectonics 18, 929-949.

80. Searle, M.P., Parrish, R.R., Thow, A., Noble, S., Phillips, R., Waters, D., 2010. Anatomy, age and evolution of a collisional mountain belt: the Baltoro granite batholith and Karakoram Metamorphic Complex, Pakistani Karakoram. Journal of the Geological Society 167, 183-202.

81. Searle, M.P., Tirrul, R., 1991. Structural and thermal evolution of the Karakoram crust. Journal of the Geological Society 148, 65-82.

82. Searle, M.P., Windley, B., Coward, M., Cooper, D., Rex, A., Rex, D., Tingdong, L., Xuchang, X., Jan, M.Q., Thakur, V., 1987. The closing of Tethys and the tectonics of the Himalaya. Geological Society of America Bulletin 98, 678-701.

83. Searle, M.P., 1991. Geology and tectonics of the Karakoram Mountains. John Wiley & Sons Inc.

84. Searle, M.P., Weinberg, R.E and Dunlap, W. J., 1998. Transpressional tectonics along the Karakoram fault zone, northern Ladakh: constraints on Tibetan extrusion. In: Holdsworth, R.E., Strachan, R.A. and Dewey, J. E (eds) 1998. Continental Transpressional and Transtensional Tectonics. Geological Society, London, Special Publications, 135, 307-326.

85. Sen, K., Mukherjee, B.K., Collins, A.S., 2014. Interplay of deformation and magmatism in the Pangong Transpression Zone, eastern Ladakh, India:

Implications for remobilization of the trans-Himalayan magmatic arc and initiation of the Karakoram Fault. Journal of Structural Geology 62, 13-24.

86. Şengör, A.C., 1984. The Cimmeride orogenic system and the tectonics of Eurasia. Geological Society of America Special Papers 195, 1-74.

87. Singh, S., Kumar, R., Barley, M.E., Jain, A., 2007. SHRIMP U–Pb ages and depth of emplacement of Ladakh Batholith, Eastern Ladakh, India. Journal of Asian Earth Sciences 30, 490-503.

88. Sláma, J., Košler, J., Condon, D.J., Crowley, J.L., Gerdes, A., Hanchar, J.M., Horstwood, M.S., Morris, G.A., Nasdala, L., Norberg, N., 2008. Plešovice zircon—a new natural reference material for U–Pb and Hf isotopic microanalysis. Chemical Geology 249, 1-35.

89. Smith, H.A., Chamberlain, C.P., Zeitler, P.K., 1994. Timing and duration of Himalayan metamorphism within the Indian plate, northwest Himalaya, Pakistan. The Journal of Geology, 493-508.

90. St-Onge, M.R., Rayner, N., Searle, M.P., 2010. Zircon age determinations for the Ladakh batholith at Chumathang (Northwest India): implications for the age of the India–Asia collision in the Ladakh Himalaya. Tectonophysics 495, 171-183.

91. Sun, X., Li, C.a., Kuiper, K., Zhang, Z., Gao, J., Wijbrans, J., 2016. Human impact on erosion patterns and sediment transport in the Yangtze River. Global and Planetary Change 143, 88-99.

92. Tapponnier, P., Peltzer, G., Le Dain, A., Armijo, R., Cobbold, P., 1982. Propagating extrusion tectonics in Asia: new insights from simple experiments with plasticine. Geology 10, 611-616.

93. Treloar, P.J., 1997. Thermal controls on early-Tertiary, short-lived, rapid regional metamorphism in the NW Himalaya, Pakistan. Tectonophysics 273, 77-104.

94. Treloar, P.J., Izatt, C.N., 1993. Tectonics of the Himalayan collision between the Indian plate and the Afghan block: A synthesis. Geological Society, London, Special Publications 74, 69-87.

95. Treloar, P.J., Rex, D., Guise, P., Coward, M., Searle, M., Windley, B., Petterson, M., Jan, M.Q., Luff, I., 1989. K-Ar and Ar-Ar geochronology of the Himalayan collision in NW Pakistan: Constraints on the timing of suturing, deformation, metamorphism and uplift. Tectonics 8, 881-909.

96. Upadhyay, R., Frisch, W., Siebel, W., 2008. Tectonic implications of new U–Pb zircon ages of the Ladakh batholith, Indus suture zone, northwest Himalaya, India. Terra Nova 20, 309-317.

97. Van Der Beek, P., Van Melle, J., Guillot, S., Pêcher, A., Reiners, P.W., Nicolescu, S., Latif, M., 2009. Eocene Tibetan plateau remnants preserved in the northwest Himalaya. Nature Geoscience 2, 364-368.

98. van Hinsbergen, D.J., Lippert, P.C., Dupont-Nivet, G., McQuarrie, N., Doubrovine, P.V., Spakman, W., Torsvik, T.H., 2012. Greater India Basin hypothesis and a two-stage Cenozoic collision between India and Asia. Proceedings of the National Academy of Sciences 109, 7659-7664.

99. Vermeesch, P., 2012. On the visualisation of detrital age distributions. Chemical Geology 312, 190-194.

100. Vermeesch, P., 2013. Multi-sample comparison of detrital age distributions. Chemical Geology 341, 140-146.

101. Wallis, D., Carter, A., Phillips, R.J., Parsons, A.J., Searle, M.P., 2016. Spatial variation in exhumation rates across Ladakh and the Karakoram: New apatite fission track data from the Eastern Karakoram, NW India. Tectonics 35, 704-721.

102. Weinberg, R., Dunlap, W., Whitehouse, M., 2000. New field, structural and geochronological data from the Shyok and Nubra valleys, northern Ladakh: linking Kohistan to Tibet. Geological Society, London, Special Publications 170, 253-275.

103. White, L., Ahmad, T., Ireland, T., Lister, G., Forster, M., 2011. Deconvolving episodic age spectra from zircons of the Ladakh Batholith, northwest Indian Himalaya. Chemical Geology 289, 179-196.

104. Wiedenbeck, M., Hanchar, J.M., Peck, W.H., Sylvester, P., Valley, J., Whitehouse, M., Kronz, A., Morishita, Y., Nasdala, L., Fiebig, J., 2004. Further characterisation of the 91500 zircon crystal. Geostandards and Geoanalytical Research 28, 9-39.

105. Wijbrans, J., Pringle, M., Koppers, A., Scheveers, R., 1995. Argon geochronology of small samples using the Vulkaan argon laserprobe, Proceedings of the Royal Netherlands Academy of Arts and Sciences, pp. 185-218.

106. Willett, S.D., Brandon, M.T., 2013. Some analytical methods for converting thermochronometric age to erosion rate. Geochemistry, Geophysics, Geosystems 14, 209-222.

107. Wittlinger, G., Vergne, J., Tapponnier, P., Farra, V., Poupinet, G., Jiang, M., Su, H., Herquel, G., Paul, A., 2004. Teleseismic imaging of subducting lithosphere

and Moho offsets beneath western Tibet. Earth and Planetary Science Letters 221, 117-130.

108. Zanchi, A., Gaetani, M., 2011. The geology of the Karakoram range, Pakistan: the new 1: 100,000 geological map of Central-Western Karakoram. Italian journal of geosciences 130, 161-262.

109. Zanchi, A., Poli, S., Fumagalli, P., Gaetani, M., 2000. Mantle exhumation along the Tirich Mir Fault Zone, NW Pakistan: pre-mid-Cretaceous accretion of the Karakoram terrane to the Asian margin. Geological Society, London, Special Publications 170, 237-252.

110. Zeitler, P.K., Chamberlain, C.P., 1991. Petrogenetic and tectonic significance of young leucogranites from the northwestern Himalaya, Pakistan. Tectonics 10, 729-741.

111. Zeitler, P.K., Meltzer, A.S., Koons, P.O., Craw, D., Hallet, B., Chamberlain, C.P., Kidd, W.S., Park, S.K., Seeber, L., Bishop, M., 2001. Erosion, Himalayan geodynamics, and the geomorphology of metamorphism. GSA Today 11, 4-9.

112. Zeitler, P.K., 1985. Cooling history of the NW Himalaya, Pakistan. Tectonics 4, 127-151.

113. Zhuang, G., Najman, Y., Guillot, S., Roddaz, M., Antoine, P.-O., Métais, G., Carter, A., Marivaux, L., Solangi, S.H., 2015. Constraints on the collision and the pre-collision tectonic configuration between India and Asia from detrital geochronology, thermochronology, and geochemistry studies in the lower Indus basin, Pakistan. Earth and Planetary Science Letters 432, 363-373.

Table 1. Sample collection site coordinates, drainage, and tectonic terranes.

Sample	Drainage	Sourced terrane	Latitude	Longitude
MRS 3	Hunza River	Karakoram, Pamir	36.3119	74.6916
MRS 4	Ghizar-Gilgit River	Karakoram, N Kohistan	35.9252	74.2656
MRS 2	Gilgit River	N Kohistan, Karakoram	35.8998	74.3968
MRS 5	Chitral River	Karakoram, Hindu Kush, Kohistan	35.6211	71.7967
MRS 8	Dir River	Kohistan	35.1427	71.9018
MRS 9	Kabul River	Swat Himalaya, Kohistan, Hindu Kush	34.1648	71.5927

Table 2. Comparison of methods for the inversion of detrital thermochronometer ages to erosion rates

<table>
<tr><th>Inversion methods</th><th>Method-1</th><th>Method-2</th><th>Method-3</th><th>Method-4</th></tr>
<tr><td rowspan="4">Common assumptions</td><td colspan="4">1. Vertical particle trajectory (no lateral variation)</td></tr>
<tr><td colspan="4">2. Representative sampling (lithology control on detrital crystal yield)</td></tr>
<tr><td colspan="4">3. Brief residence time in the sediment-transport system</td></tr>
<tr><td colspan="4">4. Cooling caused by erosion not due to tectonic exhumation (e.g. normal faulting)</td></tr>
<tr><td rowspan="2">Characters of modeled erosion rate</td><td>Temporally averaged (steady state)</td><td>Temporally averaged (steady state)</td><td>Temporally varying</td><td>Temporally averaged (steady state)</td></tr>
<tr><td>Basin-wide uniform</td><td>Basin-wide uniform</td><td>Basin-wide uniform</td><td>Spatially varying</td></tr>
<tr><td rowspan="2">Calculation of erosion rates</td><td colspan="3">Using elevation-age relation</td><td rowspan="2">Erosion-dependence of timing of particle passage from closure isotherm to surface</td></tr>
<tr><td>Mean elevation and age (point-point)</td><td>Range of elevations and ages</td><td>Piecewise (segment) elevation-age</td></tr>
<tr><td>Drainage size explored</td><td>Small</td><td>Small</td><td>Large</td><td>Large</td></tr>
<tr><td>Suitable thermochronometers</td><td>$^{40}Ar/^{39}Ar$</td><td>$^{40}Ar/^{39}Ar$</td><td>Apatite U-Th/He & Apatite fission track (encouraged for $^{4}He/^{3}He$, $^{40}Ar/^{39}Ar$)</td><td>Apatite U-Th/He, apatite fission track, ziron U-Th/He, zircon fission track, $^{40}Ar/^{39}Ar$</td></tr>
<tr><td>Reference</td><td>Brewers et al., 2003; 2006</td><td>Hodges et al., 2005; Ruhl and Hodges, 2005</td><td>Duvall et al., 2012; Avdeev et al., 2011</td><td>Brandon et al., 1998; Garver and Brandon, 1999; Willett & Brandon, 2013</td></tr>
</table>

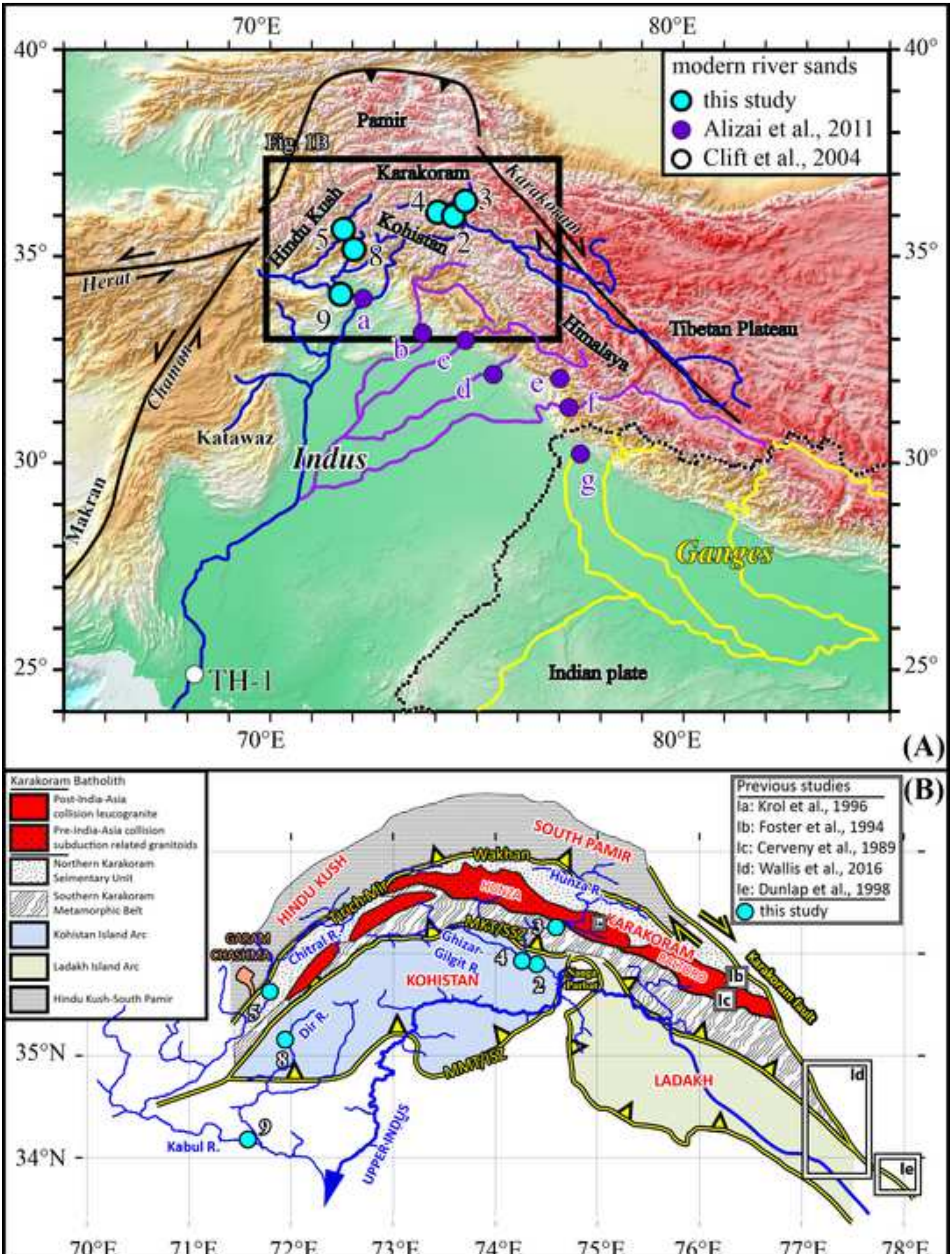
70°E
80°E
40°
35°
30°
25°
modern river sands
this study
Alizai et al., 2011
Clift et al., 2004
Pamir
Fig. 1B
Karakoram
Hindu Kush
Kohistan
Karakoram
Himalaya
Tibetan Plateau
Herat
Chaman
Katawaz
Makran
Indus
Ganges
Indian plate
TH-1
(A)
(B)
Karakoram Batholith
Post-India-Asia collision leucogranite
Pre-India-Asia collision subduction related granitoids
Northern Karakoram Selmentary Unit
Southern Karakoram Metamorphic Belt
Kohistan Island Arc
Ladakh Island Arc
Hindu Kush-South Pamir
Previous studies
Ia: Krol et al., 1996
Ib: Foster et al., 1994
Ic: Cerveny et al., 1989
Id: Wallis et al., 2016
Ie: Dunlap et al., 1998
this study
SOUTH PAMIR
HINDU KUSH
Wakhan
Hunza R.
KARAKORAM
KOHISTAN
LADAKH
Chitral R.
Ghizar-Gilgit R.
Dir R.
Kabul R.
UPPER INDUS
MMT/ISZ
Karakoram fault
70°E
71°E
72°E
73°E
74°E
75°E
76°E
77°E
78°E
35°N
34°N

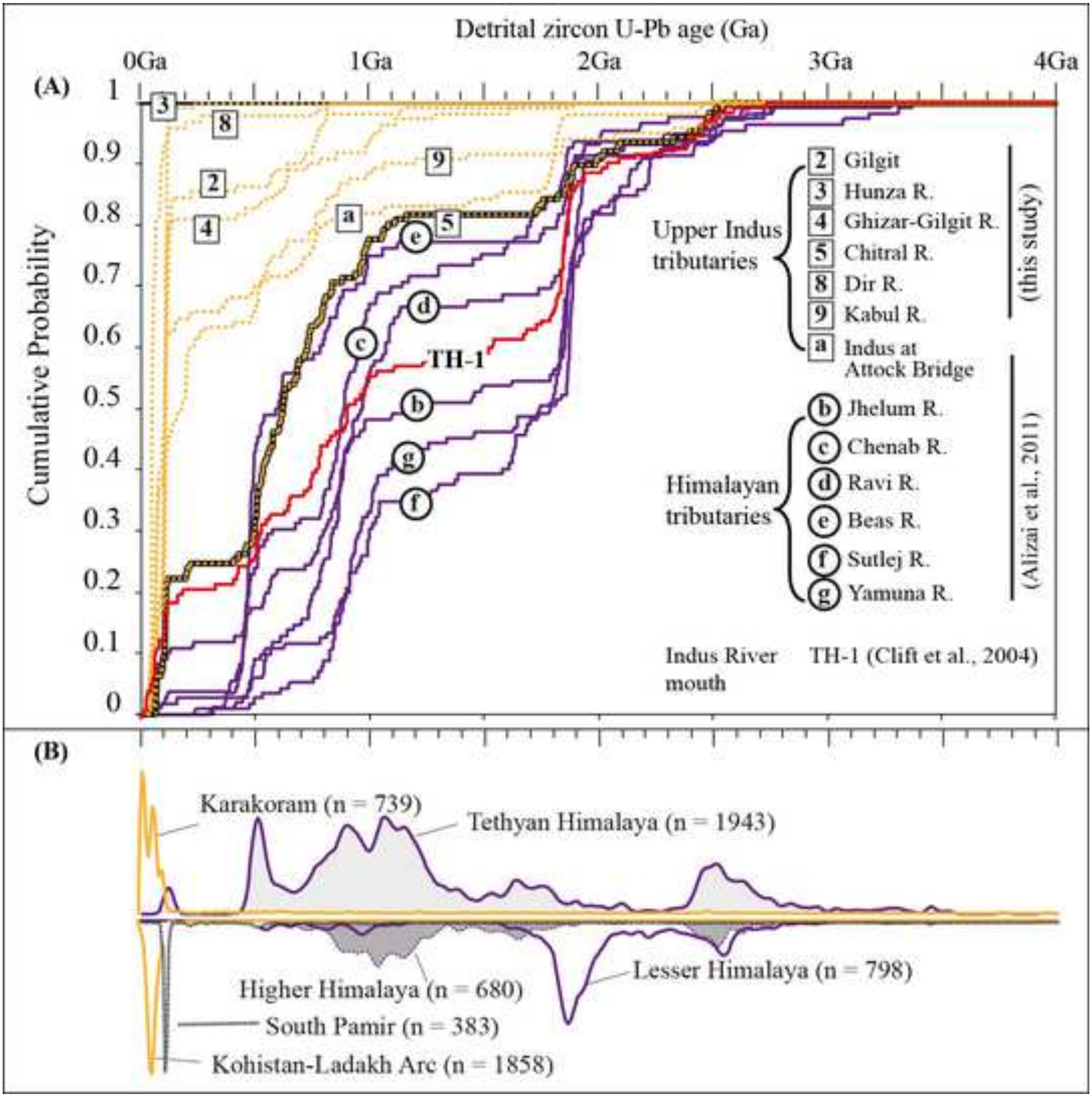
Detrital zircon U-Pb age (Ga)
0Ga
1Ga
2Ga
3Ga
4Ga
(A)
Cumulative Probability
TH-1
Upper Indus tributaries
2 Gilgit
3 Hunza R.
4 Ghizar-Gilgit R.
5 Chitral R.
8 Dir R.
9 Kabul R.
a Indus at Attock Bridge
(this study)
Himalayan tributaries
b Jhelum R.
c Chenab R.
d Ravi R.
e Beas R.
f Sutlej R.
g Yamuna R.
(Alizai et al., 2011)
Indus River mouth
TH-1 (Clift et al., 2004)
(B)
Karakoram (n = 739)
Tethyan Himalaya (n = 1943)
Lesser Himalaya (n = 798)
Higher Himalaya (n = 680)
South Pamir (n = 383)
Kohistan-Ladakh Arc (n = 1858)

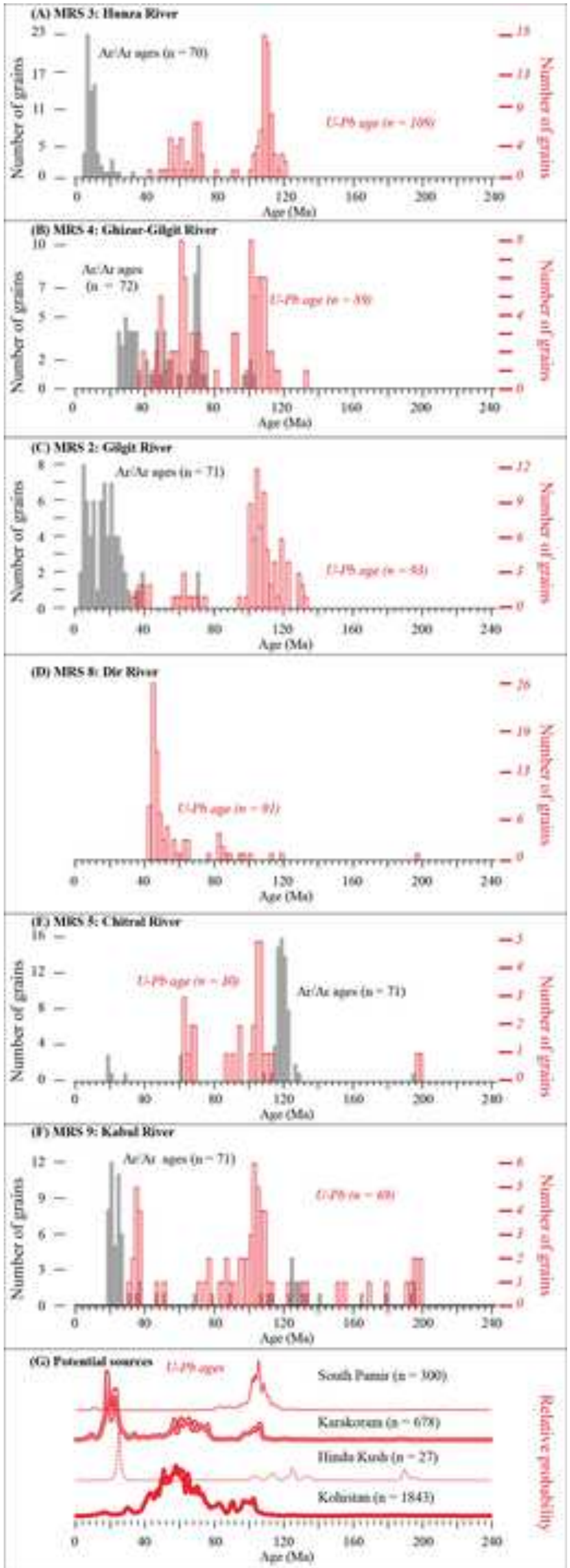
(A) MRS 3: Hunza River
(B) MRS 4: Ghizar-Gilgit River
(C) MRS 2: Gilgit River
(D) MRS 8: Dir River
(E) MRS 5: Chitral River
(F) MRS 9: Kabul River
(G) Potential sources
South Pamir (n = 300)
Karakoram (n = 678)
Hindu Kush (n = 27)
Kohistan (n = 1843)
Number of grains
Relative probability
Age (Ma)

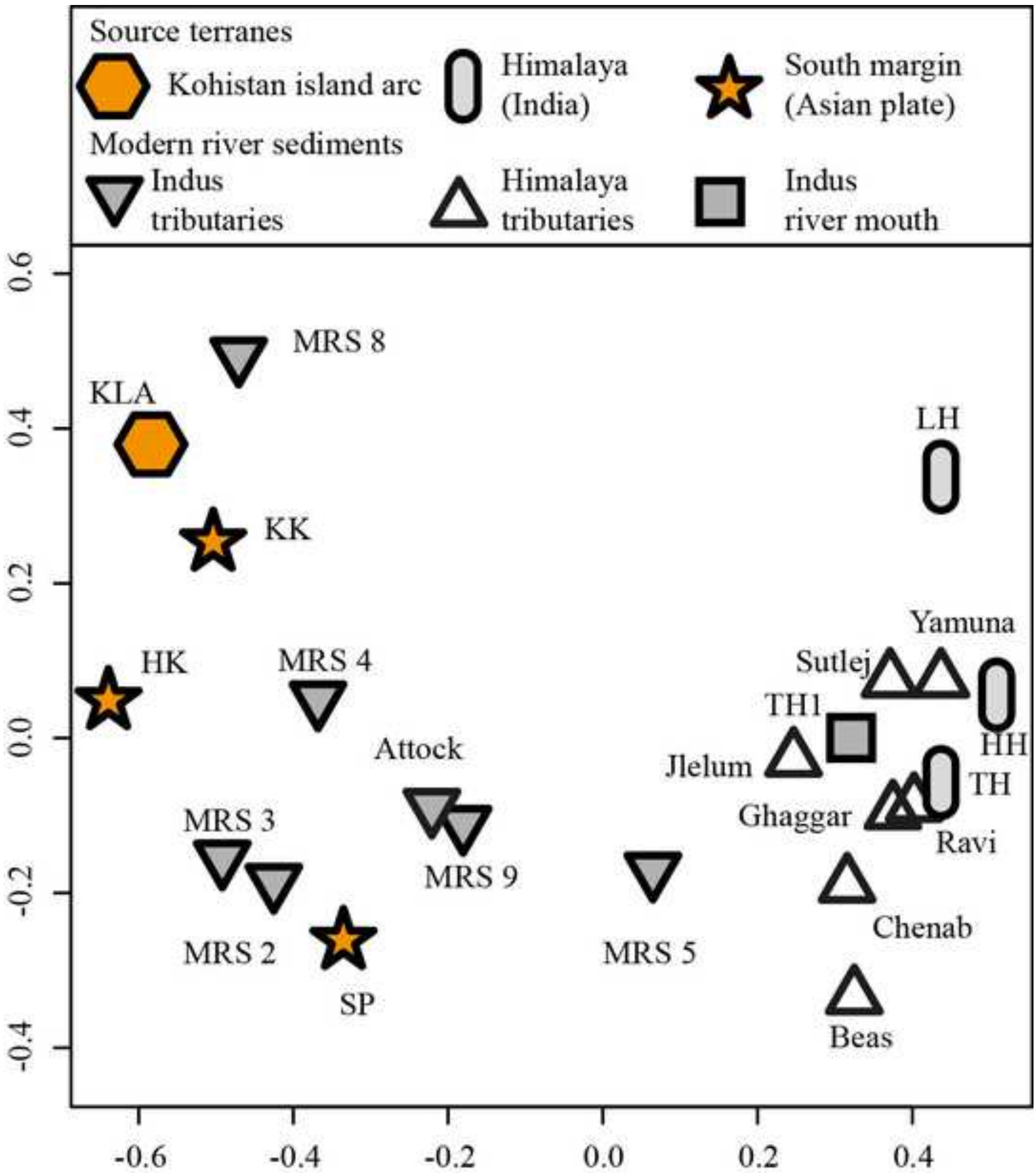

Source terranes
Kohistan island arc
Himalaya (India)
South margin (Asian plate)
Modern river sediments
Indus tributaries
Himalaya tributaries
Indus river mouth
MRS 8
KLA
KK
HK
MRS 4
Attock
MRS 3
MRS 2
SP
MRS 9
MRS 5
LH
Yamuna
Sutlej
TH1
Jlelum
HH
TH
Ghaggar
Ravi
Chenab
Beas
0.6
0.4
0.2
0.0
-0.2
-0.4
-0.6
-0.4
-0.2
0.0
0.2
0.4

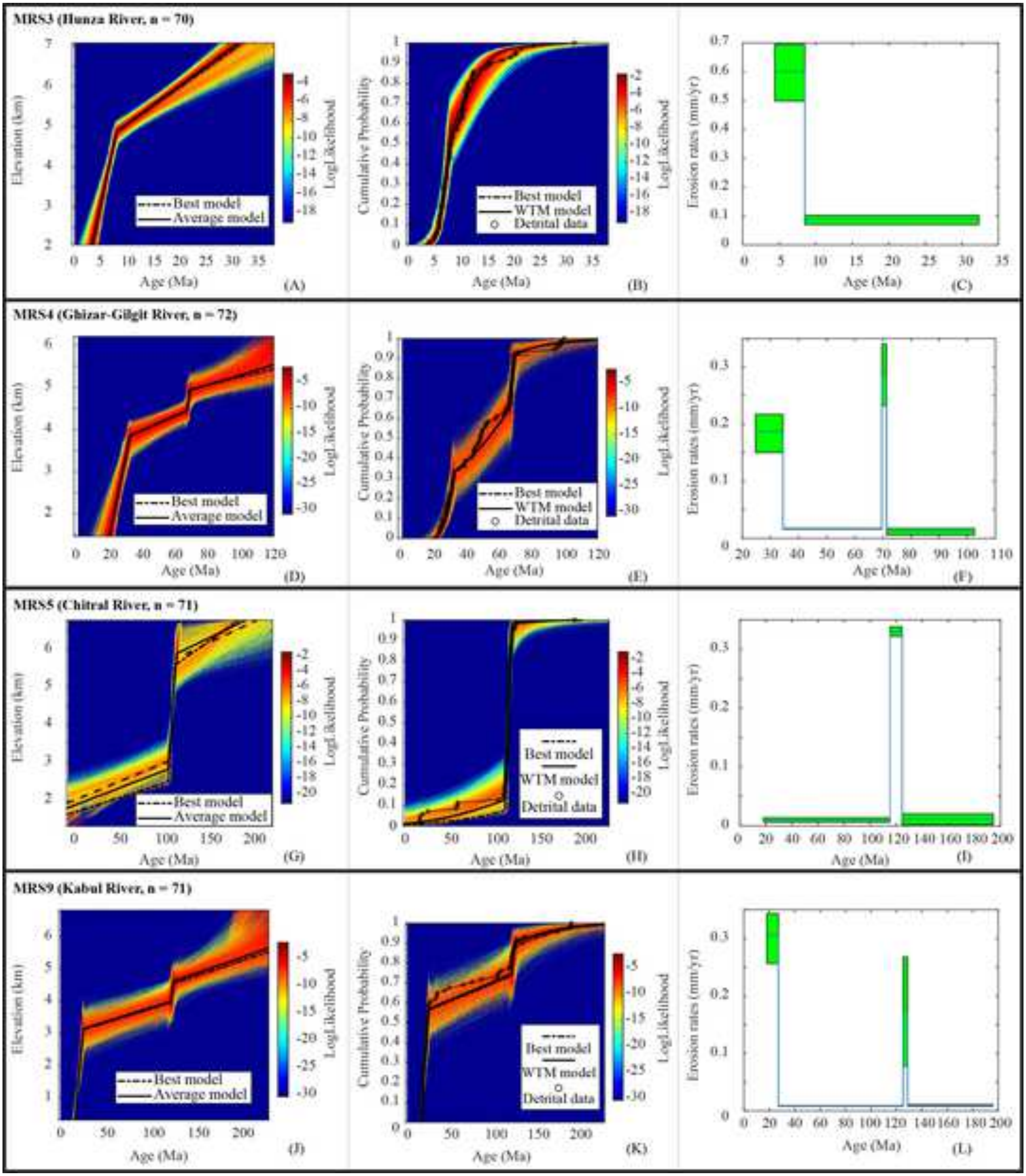

MRS3 (Hunza River, n = 70)
Elevation (km)
Age (Ma)
Best model
Average model
LogLikelihood
(A)
Cumulative Probability
Best model
WTM model
Detrital data
(B)
Erosion rates (mm/yr)
(C)
MRS4 (Ghizar-Gilgit River, n = 72)
(D)
(E)
(F)
MRS5 (Chitral River, n = 71)
(G)
(H)
(I)
MRS9 (Kabul River, n = 71)
(J)
(K)
(L)

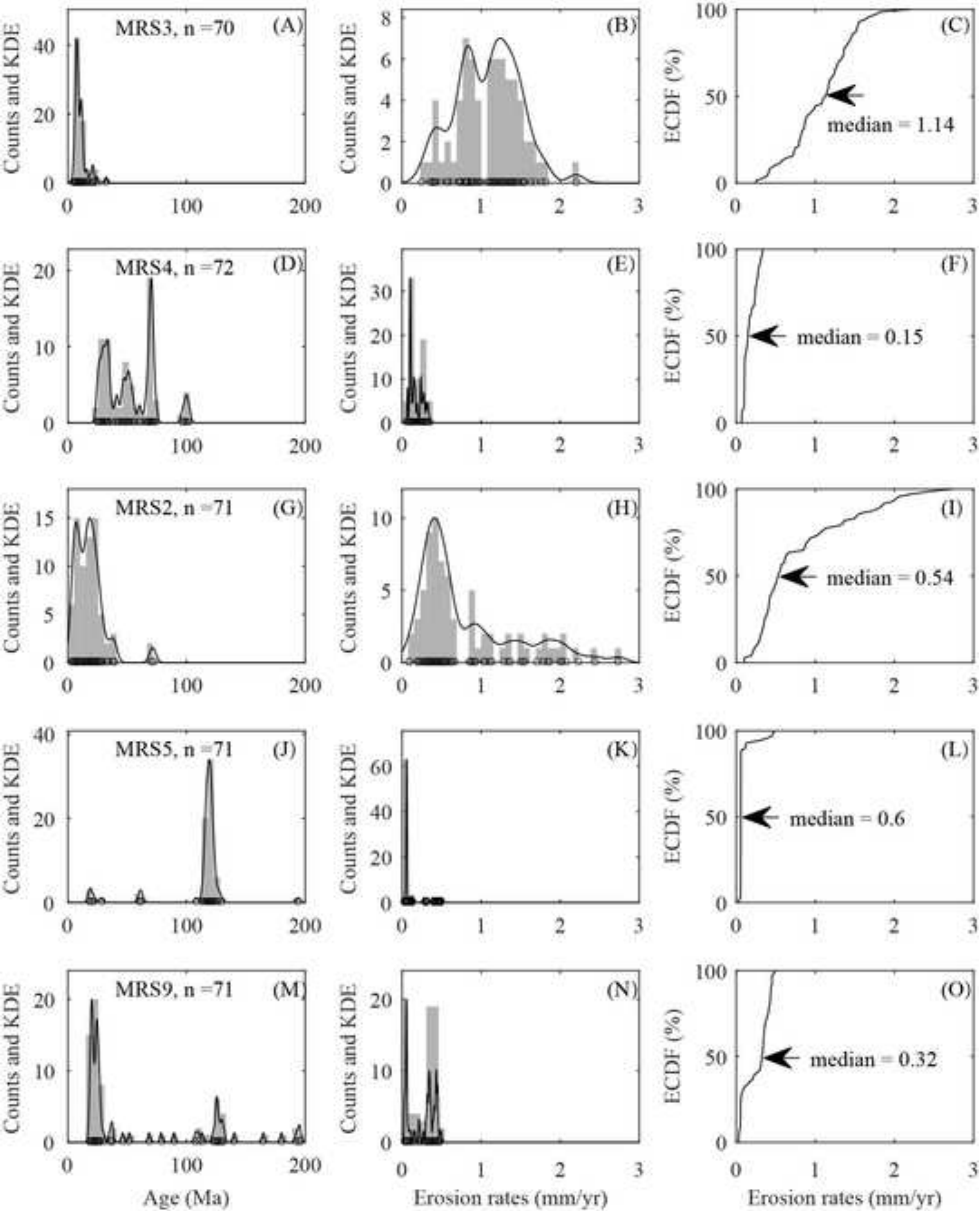

MRS3, n =70
(A)
(B)
(C)
median = 1.14
MRS4, n =72
(D)
(E)
(F)
median = 0.15
MRS2, n =71
(G)
(H)
(I)
median = 0.54
MRS5, n =71
(J)
(K)
(L)
median = 0.6
MRS9, n =71
(M)
(N)
(O)
median = 0.32
Counts and KDE
ECDF (%)
Age (Ma)
Erosion rates (mm/yr)

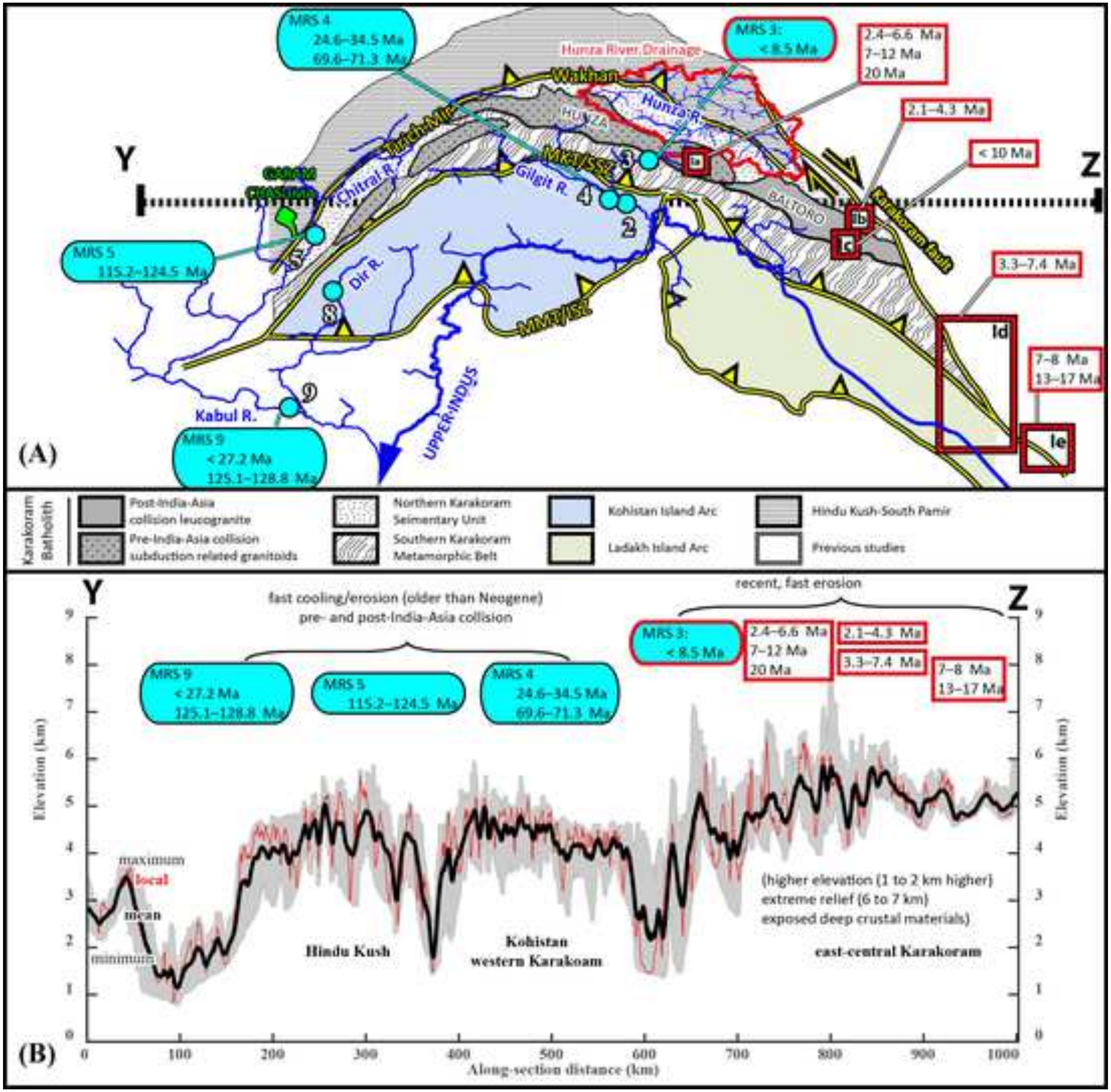
MRS 4
24.6–34.5 Ma
69.6–71.3 Ma
MRS 3:
< 8.5 Ma
Hunza River Drainage
2.4–6.6 Ma
7–12 Ma
20 Ma
2.1–4.3 Ma
< 10 Ma
3.3–7.4 Ma
7–8 Ma
13–17 Ma
Wakhan
HUNZA
Hunza R.
Tirich Mir
MKT/SSZ
Gilgit R.
Chitral R.
Dir R.
Kabul R.
UPPER INDUS
MMT/ISZ
BALTORO
Karakoram fault
Y
Z
MRS 5
115.2–124.5 Ma
MRS 9
< 27.2 Ma
125.1–128.8 Ma
Ia
Ib
Ic
Id
Ie
(A)
Karakoram Batholith
Post-India-Asia collision leucogranite
Pre-India-Asia collision subduction related granitoids
Northern Karakoram Seimentary Unit
Southern Karakoram Metamorphic Belt
Kohistan Island Arc
Ladakh Island Arc
Hindu Kush-South Pamir
Previous studies
fast cooling/erosion (older than Neogene)
pre- and post-India-Asia collision
recent, fast erosion
maximum
local
mean
minimum
Hindu Kush
Kohistan
western Karakoam
(higher elevation (1 to 2 km higher)
extreme relief (6 to 7 km)
exposed deep crustal materials)
east-central Karakoram
Elevation (km)
Along-section distance (km)
(B)